# Active Retrofit of Shear Critical RC Components Using Self-Prestressing Iron-Based Shape Memory Alloys

by

Miguel González Góez

A thesis

presented to the University of Waterloo

in fulfillment of the

thesis requirement for the degree of

Master of Applied Sciences

in

Civil Engineering

Waterloo, Ontario, Canada, 2023

© Miguel González Góez 2023

## Author’s Declaration

I hereby declare that I am the sole author of this thesis. This is a true copy of the thesis, including any required final revisions, as accepted by my examiners.

I understand that my thesis may be made electronically available to the public.

# Abstract

With growing traffic demands and structural degradation accelerated by climate change, there is a critical need for continued advancement of concrete repair and strengthening technologies to enable extended bridge service life. Specifically, transitioning to cost-effective reinforced concrete (RC) retrofit strategies that further enhance durability under service loading conditions and minimize damage development under extreme hazard conditions, which are more probable to occur in longer-lasting concrete structures, are key elements of next-generation concrete bridges.

This thesis explores the use of iron-based shape memory alloys (Fe-SMAs) as an active shear retrofit strategy for RC components. SMAs are a class of smart materials with the unique property of the shape memory effect, allowing them to fully recover plastic deformations when subsequently heated. By installing pre-strained Fe-SMA strips and activating the shape memory effect, an active pressure can be introduced to help close cracks and apply a confining stress in the concrete. The primary objective is to evaluate the performance and practicality of Fe-SMA as an active shear strengthening technique in comparison to traditional methods such as external steel reinforcement and fibre-reinforced polymer (FRP) composites.

The experimental phase of this study involved conducting push-off tests on RC specimens retrofitted with pre-deformed Fe-SMA strips. The goal was to assess the efficiency of active shear retrofitting. Additionally, finite element analysis (FEA) simulations were employed to model Fe SMA-retrofitted RC structures and investigate their behaviour under shear loading conditions. Key findings indicate that Fe-SMA retrofits, through transverse prestressing as part of the active retrofit strategy, contributed to notable improvements in the stiffness and strength of damaged RC components. Similar to passive retrofit methods, increased shear capacity was observed with higher levels of transverse reinforcement. Notably, combinations of substantial shear reinforcement ratios and elevated transverse prestressing provided the most significant gains in shear strength. Furthermore, the addition of prestressed Fe-SMA retrofits was found to effectively reduce shear crack widths and mitigate the progression of subsequent shear crack width growth.

This study not only demonstrates the potential of Fe-SMA as a promising solution for active shear strengthening but also contributes to the development of future field-scale tests. The presence of Fe-SMA in damaged structures offers the prospect of multiple improvements, marking a significant advancement in the field of shear retrofitting.

# Acknowledgements

The completion of this journey has been made possible through the support and encouragement of numerous individuals. First and foremost, I would like to thank my supervisors, Drs. Trevor Hrynyk and Eugene Kim for your guidance and support throughout the last 2 years. Your expertise and commitment to my academic and professional development have been invaluable.

I would like to express my gratitude to my family. To my parents and my brother for their unwavering support and encouragement during my entire life. To my partner Mishell, for all your love and understanding during these years.

The academic journey is often made more meaningful through collaboration and shared ideas. I extend my thanks to my colleagues and fellow graduate students who have engaged in fruitful discussions, provided encouragement, and offered their expertise.

I am thankful to Colfuturo and Sapiencia for their financial support. Your support has allowed me to pursue this research with dedication and focus.

Last but certainly not least, I would like to acknowledge the staff at the structures laboratory, Isabelle Graansma, Robert Kaptein and Peter Volcic for their assistance and providing an enriching environment for research.

# Dedication

To my niece Alma and to the memory of my elder brother Alexis.

# Table of Contents

Author's Declaration ..... ii

Abstract ..... iii

Acknowledgements ..... iv

Dedication ..... v

List of Figures ..... ix

List of Tables ..... xi

List of Abbreviations ..... xii

Chapter 1 Introduction ..... 1

1.1 General ..... 1

1.2 Research Needs ..... 2

1.3 Objectives ..... 3

1.4 Thesis Organization ..... 4

Chapter 2 Literature Review ..... 5

2.1 General ..... 5

2.2 Concrete Under Shear ..... 5

2.2.1 Shear Damage ..... 6

2.2.2 Shear Design and Analysis ..... 7

2.2.3 Push-off Tests ..... 11

2.3 Shear Retrofit Techniques ..... 13

2.3.1 Addition of Steel Reinforcement ..... 13

2.3.2 Addition of Fibre-Reinforced Polymer Strengthening ..... 15

2.3.3 Concrete Jacketing ..... 18

2.4 Shape Memory Alloys ..... 19

2.4.1 Background: ..... 19

2.4.2 Properties: 20
2.4.3 Composition and Commercially Available SMAs: 22
2.4.4 Fe-SMA Applications in RC Structures: 25
2.5 Fe-SMA Shear Strengthening 28
2.6 Summary 30
Chapter 3 Finite Element Modelling 31
3.1 General 31
3.2 Preliminary Validation and Benchmark Analysis 31
3.2.1 Modelling Approach 33
3.2.2 Validation for Benchmark RC Beam 34
3.3 Parametric Study 35
3.4 Results and Discussion 37
3.4.1 Shear Response 37
3.4.2 Crack Closing Potential 40
3.5 Summary 42
Chapter 4 Experimental program 43
4.1 General 43
4.2 Material Characterization 43
4.2.1 Concrete Mixture 44
4.2.2 Steel Reinforcement 45
4.2.3 Fe-SMA strips 47
4.3 Recovery Stress Tests 48
4.4 Push-Off Tests 49
4.4.1 Test Specimen 50
4.4.2 Test Matrix 52

4.4.3 Test Setup and Instrumentation ..... 53
4.4.4 Test Procedure ..... 54
Chapter 5 Experimental Results and Discussion ..... 59
5.1 General ..... 59
5.2 Recovery Stress Results ..... 59
5.3 Push-Off Results ..... 60
5.3.1 Peak Load ..... 62
5.3.2 Shear Stress – Slip ..... 64
5.3.3 Shear Stress – Crack Width ..... 65
5.3.4 Self-Prestressing and Shear Behaviour Enhancement ..... 66
Chapter 6 Conclusions and Recommendations ..... 67
6.1 General Remarks ..... 67
6.2 Recommendations for Future Work ..... 68
References ..... 69
Appendix A Material characterization results ..... 76

# List of Figures

Figure 1.1. RC push-off specimens with external Fe-SMA retrofit ..... 3
Figure 2.1. Shear failure of pier wall of the Wu-Shi Bridge, Taiwan (Sung et al., 2009) ..... 6
Figure 2.2. Mörsch's truss analogy model (Grandić et al., 2015) ..... 8
Figure 2.3. Eurocode 2 strut-and-tie-model for RC elements (Maitenaz et al., 2020) ..... 9
Figure 2.4. Nature of disturbed stress fields in cracked RC (Vecchio, 2000) ..... 10
Figure 2.5. Saw and tooth model (Santos & Júlio, 2012) ..... 11
Figure 2.6. Displacements and stresses on the shear plane in push-off specimens (Echegaray-Oviedo et al., 2017) ..... 12
Figure 2.7. Steel strap and plate arrangements (Altin et al., 2005) ..... 14
Figure 2.8. Installation of the NSM CFRP rod (Al-Mahmoud et al., 2015) ..... 16
Figure 2.9. CFRP external reinforcement on wide-webbed RC beam (Shekarchi, 2016) ..... 17
Figure 2.10. Jacketed beams (dimensions in mm) (Chalioris & Pourzitidis, 2012) ..... 19
Figure 2.11. Stress-strain-temperature diagram of SMA adopted from (Zareie et al., 2020) ..... 21
Figure 2.12. Fe-SMA prestressing concept (González-Góez et al., 2023) ..... 24
Figure 2.13. RC beam strengthened with NSM Fe-SMA strips (Shahverdi et al., 2016) ..... 25
Figure 2.14. Fe-SMA strengthened RC slab (Schranz et al., 2021) ..... 27
Figure 2.15. Fe-SMA rods for enhancement of shear resistance (Soroushian et al., 2001) ..... 27
Figure 2.16. Fe-SMA strengthened beam (Cladera et al., 2020) ..... 29
Figure 2.17. Fe-SMA shear strengthening with spray mortar (Czaderski et al., 2021) ..... 29
Figure 2.18. Beam with activated Fe-SMA strips (Montoya-Coronado et al., 2019) ..... 30
Figure 3.1. Jirsa et al. (2017) double-curvature control beam ..... 33
Figure 3.2. VecTor2 two-dimensional model ..... 33
Figure 3.3. Results for Jirsa et al. (2017) RC Control Beam ..... 34
Figure 3.4. NLFEA loading phases. ..... 36
Figure 3.5. VecTor2 mesh with smeared Fe-SMA retrofit. ..... 36
Figure 3.6. Fe-SMA stress-strain response (K. Hong et al., 2018) ..... 37
Figure 3.7. Shear response ..... 38
Figure 3.8. Influence of prestressing level (VN seed model) ..... 40
Figure 3.9. Crack width in a single element ..... 41
Figure 3.10. Crack widths in test span before prestressed Fe-SMA addition ..... 42
Figure 4.1. Tensile test on reinforcement bars ..... 46

Figure 4.2. Fe-SMA tensile test specimen (dimensions in mm) ..... 47
Figure 4.3. Fe-SMA tensile test setup ..... 48
Figure 4.4. Recovery stress test phases ..... 48
Figure 4.5. Recovery stress test setup ..... 49
Figure 4.6. Push-off specimen ..... 50
Figure 4.7. Push-off specimen details ..... 51
Figure 4.8. Rebar cages preparation ..... 51
Figure 4.9. Instrumentation (LVDT) layout ..... 54
Figure 4.10. Precracking phase ..... 55
Figure 4.11. Fe-SMA on precracked specimens ..... 56
Figure 4.12. Push-off test setup ..... 57
Figure 4.13. Bearing surface grinding ..... 58
Figure 5.1. Recovery stress test results ..... 60
Figure 5.2. Push-off specimens ..... 61
Figure 5.3. Axial load vs measured slip results ..... 62
Figure 5.4. Shear plane after failure ..... 63
Figure 5.5. Shear stress vs slip results ..... 64
Figure 5.6. Shear stress vs crack width results ..... 65

# List of Tables

Table 3.1. Summary of parameters. ..... 35
Table 3.2. Peak shear capacities and retrofit strength gains ..... 39
Table 3.3. Peak shear capacity and influence of prestressing level ..... 40
Table 4.1. Summary of compressive test on concrete cylinders. ..... 44
Table 4.2. Material Properties of Reinforcement Steel ..... 46
Table 4.3. Material Properties of Iron-based Shape Memory Alloy ..... 48
Table 4.4. Test matrix ..... 52
Table 5.1. Recovery stress at the end of the test ..... 59
Table 5.2. Precracking loads. ..... 60
Table 5.3. Push-off peak loads ..... 62

# List of Abbreviations

| | |
|---|---|
| BCC | Body-Centered Cubic |
| BCT | Body-Centered Tetragonal |
| BRB | Buckling-Restrained Brace |
| CFRP | Carbon Fibre-Reinforced Polymer |
| DSFM | Disturbed Stress Field Model |
| FCC | Face-Centered Cubic |
| FEA | Finite Element Analysis |
| Fe-SMA | Iron-Based Shape Memory Alloys |
| FRP | Fibre-Reinforced Polymer |
| LVDT | Linear Variable Differential Transformer |
| MCFT | Modified Compression Field Theory |
| NiTi | Nickel-Titanium Alloy |
| NLFEA | Nonlinear Finite Element Analysis |
| NRCC | National Research Council Canada |
| NSM | Near-Surface Mounted |
| RC | Reinforced Concrete |
| SCC | Self-Compacting Concrete |
| SMA | Shape Memory Alloys |
| SME | Shape Memory Effect |
| UV | Ultraviolet |

# Chapter 1
# Introduction

## 1.1 General

The National Research Council Canada (NRCC) warns that more than one-third of bridges in the country are at least 40 years old (Federation of Canadian Municipalities, 2019). As these vital pieces of infrastructure age, concrete deterioration becomes a pressing concern, exacerbated by factors such as insufficient maintenance, repeated vehicular loading, severe weather conditions, and the accelerated corrosion of reinforcement due to climate change. Among the critical challenges facing concrete bridges is the degradation of reinforced concrete (RC) components, particularly their vulnerability to shear damage and failure. Retrofitting these aging bridges to enhance their shear resistance presents an engineering challenge, necessitating innovative solutions and continued advancement of concrete repair technologies.

One promising solution involves near-surface mounted (NSM) methods as an alternative for retrofitting existing RC structures (De Lorenzis & Teng, 2007). These methods entail the installation of externally bonded reinforcement to an existing element, connected via through-bolts or epoxy adhesive. NSM techniques can enhance structural load-carrying capacity, reduce cracking, and improve durability. Nevertheless, most NSM retrofit projects use passive techniques that only become engaged when the structure is further distressed from its current state. Active NSM methods, on the other hand, utilize external energy sources to create prestressing forces within the retrofitted structure, often leveraging shape memory alloys (SMAs) (Shin & Andrawes, 2010).

SMAs are noteworthy materials that exhibit a unique property known as the shape memory effect (SME). SMAs can be deformed and then returned to their original shape when subsequently heated. This inherent characteristic makes SMAs ideal for repairing shear-damaged concrete structures, as they can be easily shaped to conform to structural contours and then restored to their original form through controlled heating. Recently, researchers have developed a low-cost solution using iron-based shape memory alloys (Fe-SMAs). The strain recovery generated by the SME can produce recovery stresses exceeding 300 MPa at temperatures of around 200°C (Jeong et al., 2022) which creates self-prestressing in the structural element without the need for jacking or anchorage devices.

## 1.2 Research Needs

Concrete structures, particularly bridges, face a growing need for effective retrofit strategies to address aging and degradation. While various methods exist for enhancing the flexural performance and durability of RC members, fewer practical options are available to mitigate transverse shear damage. Current retrofit techniques primarily involve passive strategies, often relying on external reinforcement engaged only after damage occurs. Active transverse reinforcement strategies, driven by the unique properties of Fe-SMAs, have been relatively rare due to implementation complexities and durability concerns associated with external reinforcement applications.

The conventional approach to retrofitting shear-critical RC elements predominantly relies on passive strategies, such as adding external steel reinforcement or fibre-reinforced polymers (FRPs). While these methods have proven effective in enhancing the ultimate strength and ductility of structures, they present several drawbacks. Firstly, the installation of external steel reinforcement is highly invasive, necessitating extensive surface preparation and the use of large anchors. These actions may weaken the concrete and lead to structural modifications, potentially introducing unforeseen complications. Furthermore, the long-term durability of the bonding interface is a cause for concern, as environmental factors can erode the effectiveness of strengthening over time. In recent years, the adoption of FRP retrofitting for shear strengthening in RC structures has grown substantially. FRP, composed of oriented fibres embedded in a polymer matrix, offers benefits such as high strength, corrosion resistance, and lightweight properties. However, this method also confronts challenges. Proper surface preparation and bonding are essential to ensure efficient shear force transfer between the FRP and concrete, demanding meticulous surface roughening and cleaning. Additionally, the impact of environmental exposure on FRP materials raises concerns, with factors like elevated temperatures, humidity, and ultraviolet (UV) radiation potentially compromising performance and long-term durability.

To address these challenges, this research investigates the effectiveness of external prestressed Fe-SMAs in shear-critical RC members. An experimental program involving RC push-off specimens (Figure 1.1) was carried in three phases: i) pre-cracking along the shear plane, ii) retrofitting with pre-strained and activated Fe-SMAs, iii) followed by a vertical loading until failure. Additionally, field-scale specimens are modelled using VecTor2 software to assess Fe-SMA strengthening effects. This thesis aims to evaluate the Fe-SMA's potential in delaying or preventing crack propagation in concrete structures, providing valuable insights into its use as a reinforcement method.

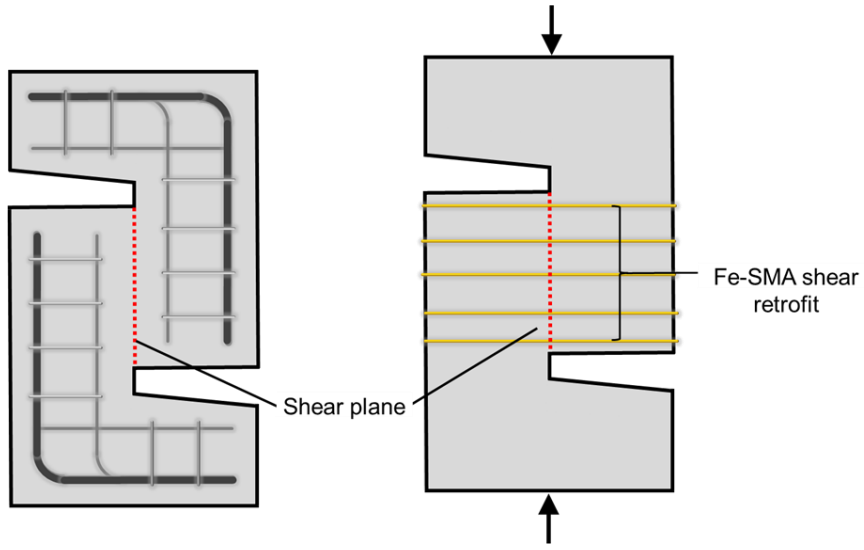



**Figure 1.1.** RC push-off specimens with external Fe-SMA retrofit

## 1.3 Objectives

The overarching aim of this study is to evaluate the performance and practicality of Fe-SMA as an active shear strengthening technique compared to traditional passive methods. For that purpose, the following research objectives have been defined:

1. Conduct tensile tests to characterize the behaviour of iron-based SMA strips and steel reinforcement with different diameters (e.g., 10M, 20M, and 3/16") to understand their mechanical properties.
2. Perform recovery stress tests on Fe-SMA strips to determine the stress recovery capacity of the material when subjected to thermal activation, with a focus on investigating the influence of different strain levels and temperature variations.
3. Carry-out push-off tests on RC specimens retrofitted with pre-deformed Fe-SMA strips to evaluate the efficacy of active shear retrofitting on shear deficient RC elements, considering different retrofit configurations.
4. Conduct finite element analysis (FEA) simulations to model SMA retrofitted RC structures and investigate their behaviour under various loading conditions. The FEA models will be validated against experimental results presented in the literature and used to gain insights into the mechanical response of the retrofitted structures.

## 1.4 Thesis Organization

This thesis is organized into six chapters to comprehensively present the research findings and discussions. Chapter 1, the current chapter, serves as an introduction, outlining the research needs and objectives of the study. Chapter 2 presents a detailed literature review on shear retrofitting methods for RC structures, including the use of FRP composites and other innovative techniques, including Fe-SMA. Chapter 3 presents the FEA models of SMA retrofitted RC structures and compares the simulation results with experimental findings. Chapter 4 describes the experimental program, including material characterization, recovery stress tests, and push-off tests, providing insights into the behaviour of Fe-SMA under various conditions. Chapter 5 presents the results of the experimental tests and discusses their implications in the context of active shear retrofitting. Finally, Chapter 6 summarizes the conclusions drawn from the study, highlighting the effectiveness of Fe-SMA as an active shear strengthening method and its potential applications in shear deficient RC structures.

# Chapter 2
# Literature Review

## 2.1 General

The purpose of this literature review is to provide an overview of the current state of knowledge on the use of shape memory alloys (SMAs) as a retrofit for shear-damaged concrete structures, identify research gaps, and provide direction for further research.

Shear damage in concrete structures refers to the degradation or failure of the concrete due to shear forces acting on the structure and can occur due to various factors such as natural disasters, aging, and overloading. The review will begin by discussing the basics of shear damage in concrete structures and the need for retrofitting. It will then provide an overview of different retrofitting techniques currently available and the advantages and disadvantages of each. The review will then focus on the behaviour of SMAs in concrete structures, including their mechanical properties and the factors that can affect their performance. Ultimately, the review will discuss the use of SMAs in concrete retrofitting and provide an overview of previous studies that have investigated the effectiveness of SMAs as a retrofit for shear-damaged concrete structures.

Overall, the literature review seeks to identify areas where further research is needed to advance the use of SMAs in concrete retrofitting. This review will provide valuable insights into the effectiveness of SMAs as a retrofitting material for concrete structures, contributing to the development of more sustainable and durable infrastructure.

## 2.2 Concrete Under Shear

Reinforced concrete (RC) is a composite material, composed of steel and concrete, which is widely used in the construction of buildings, bridges, and infrastructure. It has been used as a versatile building material since its introduction in the early 20th century. The advantages of RC include its strength, durability, affordability, and versatility. However, RC components are often subject to shearing demands which, if not accounted for properly, can cause significant damage to the structure. In this section, the effects of shear on RC and the importance of retrofitting in order to prevent such damage will be discussed.

Shear is a force that acts perpendicular to the longitudinal axis of a beam or a column (Leet et al., 2021). It can occur due to various environmental, static, or dynamic loads, such as wind, seismic activity, and vehicle traffic. In RC, shear forces are transmitted through the steel reinforcement bars (rebar) and the concrete matrix. The steel rebar provides the necessary strength to resist the tensile forces, while the concrete matrix acts as a connecting medium between the steel bars and provides compression resistance. The concrete and steel work together to resist the applied loads, but if the capacity of the reinforcing steel or concrete is exceeded, abrupt and brittle failures can occur. The shear capacity of RC elements depends on various factors such as the type and strength of the concrete, the geometry of the element, the amount and quality of the reinforcement, and loading conditions.

### 2.2.1 Shear Damage

The effects of shear damage can range from minor cracking to complete failure of the structure (Figure 2.1). Cracking in concrete due to shear damage typically occurs diagonally, forming a pattern of inclined cracks. The cracks can be narrow or wide, depending on the severity of the shear force and the detailing of the RC component. In severe cases, concrete can spall or break away from the reinforcement, exposing the steel bars and compromising the strength and durability of the structure. Shear damage can also lead to a reduction in the stiffness and ductility of the structure. The stiffness of the structure is affected as the cracks allow for additional deformation, resulting in increased deflection and drift. In addition to deformation, the structural ductility diminishes as the presence of cracks limits the structure's capacity to absorb energy, thereby increasing its likelihood of brittle failure (Fédération internationale du béton, 2010).



**Figure 2.1.** Shear failure of pier wall of the Wu-Shi Bridge, Taiwan (Sung et al., 2009)

To prevent shear damage in concrete structures, engineers use various design and construction strategies. These strategies include the use of appropriate reinforcement, the correct placement and spacing of reinforcement, the use of shear walls and other lateral load-resisting systems, and proper construction practices to ensure good concrete quality and placement. Retrofitting techniques can also be used to strengthen existing concrete structures that have experienced shear damage. These techniques include the addition of near surface mounted (NSM) steel reinforcement or FRP, and the addition of concrete jacketing. The selection of the appropriate retrofitting technique depends on several factors, such as the type and extent of damage, the structural configuration, and the budget. The mentioned techniques will be further discussed in Section 2.3.

### 2.2.2 Shear Design and Analysis

The analysis of shear in concrete is a critical aspect of designing safe and efficient concrete structures. Over the years, several models have been developed to analyze and predict the shear behaviour of RC structures. In this section, different models commonly used in the analysis of shear in RC structures will be discussed.

#### 2.2.2.1 Fixed Angle Truss Models

In fixed angle truss models RC beams are analyzed as a simple or multiple truss system, where the membrane elements are treated like struts. The basic premise of the truss model is that cracked concrete in the web of the section resists shear by a diagonal uniaxial compressive stress in a concrete strut, which pushes the flanges apart and causes tension in the stirrups that hold the section together. Therefore, the compressive strut and tension tie system resembles a truss (Figure 2.2). The Mörsch model (Mörsch, 1908) assumes that the compression strut's angle from the beam axis ($\theta$) is 45º. This assumption forms the basis of the design approach, allowing for the calculation of required forces in the shear reinforcement. This approach forms the basis of existing ACI 318 shear design calculations for beam-type members (American Concrete Institute, 2019).

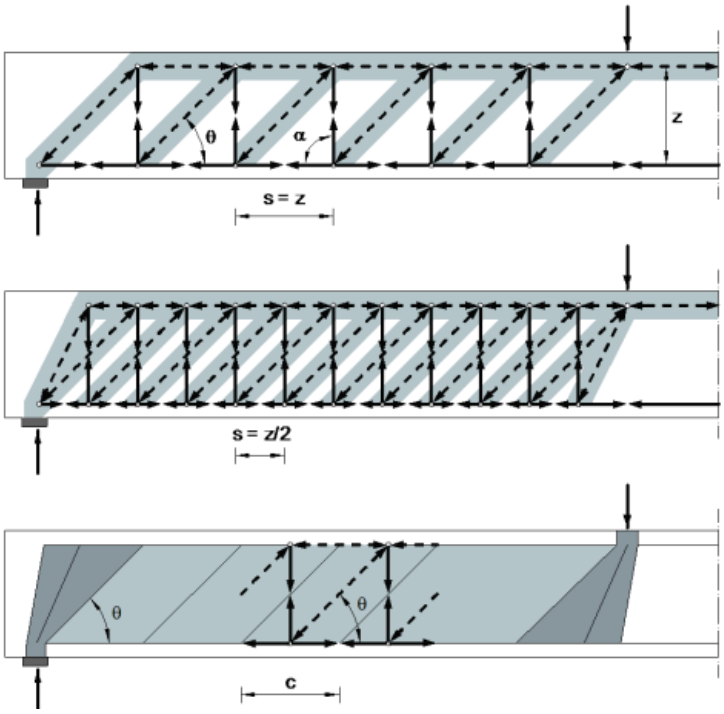



**Figure 2.2.** Mörsch's truss analogy model (Grandić et al., 2015)

#### 2.2.2.2 Variable Angle Truss Models

Another approach was introduced in 1969 (Regan, 1969) where the angle of strut inclination (θ) is not restricted to 45º. In this approach, the shear resistance is entirely based on an equivalent truss model, with no additional contribution from the concrete (Figure 2.3). However, the truss angle can be adjusted to a value within upper and lower limits, allowing for more flexibility in the design. The variable angle truss model assumes that an inclined stress field develops in the concrete at an angle θ, creating an equivalent truss with tension forces in the steel shear reinforcement, longitudinal tension in the steel reinforcement in the tension face, and compression in the concrete "compression chord" located in the compressive face. The truss forces are calculated based on the condition of equilibrium with the applied shear force, bending moment, and axial force. By limiting the truss forces to values associated with steel yielding or concrete crushing, the model can estimate the shear resistance. Examples include the current EN 1992-1-1 design procedures for RC sections in shear (European Committee for Standardization, 2004).

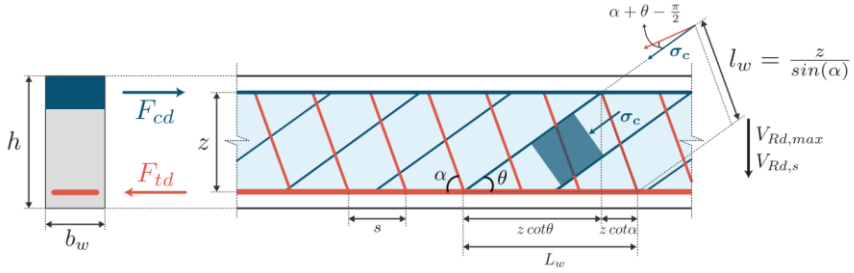



**Figure 2.3.** Eurocode 2 strut-and-tie-model for RC elements (Maitenaz et al., 2020)

#### 2.2.2.3 Compression Field/Stress Field Theories

The Modified Compression Field Theory (MCFT), developed by Vecchio & Collins in 1996, is an analytical model that treats cracked concrete as a distinct material with its own unique stress-strain characteristics. The theory formulates equilibrium, compatibility, and stress-strain relationships using average stresses and strains, while also accounting for local stress conditions at the locations of cracks. Following the development of the MCFT, the Disturbed Stress Field Model (DSFM) (Figure 2.4) was developed by Vecchio in 2000 as an extension, addressing some of the simplifying assumptions made in the formulation of MCFT. The DSFM also formulates compatibility, equilibrium, and constitutive response using average stresses and strains, while considering compression softening and tension stiffening mechanisms. In addition, the theory considers local conditions at the locations of cracks, as the presence of cracks creates disturbances in the stress fields that can influence behaviour. The key advancement of the theory is the inclusion of discrete slip deformations on the crack surfaces in the formulation of compatibility relations, negating the shear-on-the-crack checks required to account for aggregate interlock failures in MCFT.

The analytical procedure that results from the DSFM is between fixed crack models and rotating crack models, capturing the strengths of each. Unlike conventional fixed crack models, the DSFM allows for a gradual and progressive reorientation of concrete principal stress direction and crack direction, although it is delayed to a certain extent. Unlike common rotating crack models, the DSFM allows for the divergence of principal stress and principal strain directions. In both respects, this is more consistent with observed behaviour. The methods presented in this section form the basis for the General Method in CSA A23.3, CSA S6, AASHTO LRFD, and the AS5100 shear design provisions (American Association of State Highway and Transportation Officials, 2019; Canadian Standards Association, 2019a, 2019b; Standards Australia, 2017).

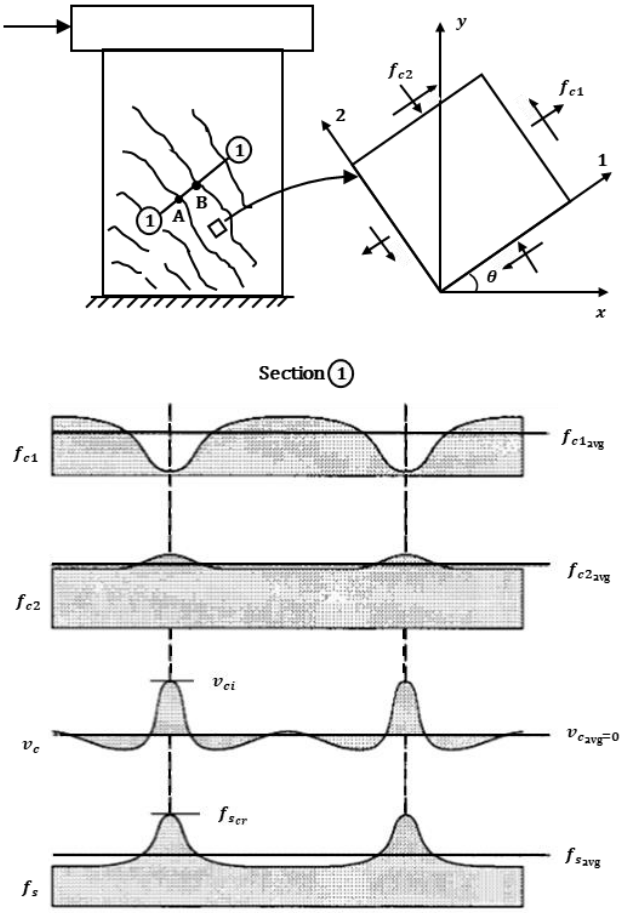



**Figure 2.4.** Nature of disturbed stress fields in cracked RC (Vecchio, 2000)

### 2.2.2.4 Shear Friction Models

Shear-friction theory serves as a valuable tool for predicting the strength of concrete-to-concrete interfaces under longitudinal shear stresses. Initially introduced in 1966, this theory has been widely adopted in design codes for RC structures, including Eurocode, ACI, CSA, AASHTO LFRD, and the PCI design handbook (American Association of State Highway and Transportation Officials, 2019; American Concrete Institute, 2019; Canadian Standards Association, 2019a; European Committee for Standardization, 2004; Precast/Prestressed Concrete Institute, 2010). It postulates that the transfer of shear forces at the concrete-to-concrete interface, experiencing simultaneous shear and compression forces, is achieved solely through friction. A simple saw-tooth model is commonly utilized to illustrate the fundamental principles of this theory (Figure 2.5), considering the influence of both reinforcement crossing the interface and external forces acting normal to the shear plane.

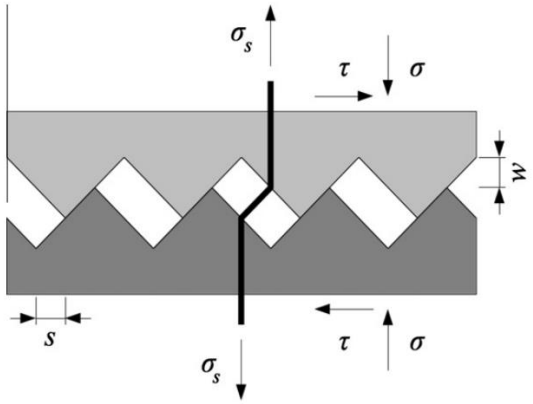



**Figure 2.5.** Saw and tooth model (Santos & Júlio, 2012)

The shear strength at the interface results from a combination of three load carrying mechanisms: adhesion, shear-friction, and shear reinforcement. Adhesion originates from chemical bond connections between concrete particles, leading to shear transfer through mechanical interlocking. Under compression, shear-friction becomes the predominant mechanism. As the relative displacement between the concrete parts increases, the reinforcement crossing the interface becomes tensioned, inducing compression and transferring shear load through friction. The shear reinforcement is also subjected to shear, known as dowel action. The 'shear-friction theory' can predict the shear strength of various concrete-to-concrete interfaces, including precast-cast-in-place interfaces, interfaces between elements cast at different times, element-support interfaces, interfaces with repairing or strengthening layers, and interfaces formed by cracks in an element (Santos & Júlio, 2012).

### 2.2.3 Push-off Tests

Research based on shear-friction models, performed mainly using different forms of push-off specimens, has provided valuable insights into the behaviour of RC under shear loads. For example, Hofbeck & Mattock (1969) showed that this theory allows conservative shear transfer strength estimations with a preexisting crack along the shear plane. Mattock & Hawkins (1972) demonstrated that the behaviour of a push-off specimen under shear loads significantly differs depending on whether the specimen has been previously precracked or not. Precracked specimens reduce ultimate shear stress and increase slip displacements compared to uncracked ones, while the behaviour in cracked specimens depends on the shear transfer mechanisms that take place at the single crack location. The push-off test has also demonstrated that the "Shear-Friction Theory" can be extended to situations in which RC lies at an arbitrary angle to the shear plane.

In the push-off test, a Z-shaped RC specimen is used, comprising two L-blocks, with the contact zone between them defined as the shear plane (Figure 2.6). The test procedure involves precracking the specimen, and then applying an external load that induces relative displacements between both sides of the crack. The vertical displacement at the crack mouth is termed slip, while the displacement normal to the shear plane is the crack width. The applied load also generates shear stress on the shear plane. Additionally, if a confinement force limits the crack width due to internal or external factors, normal stress acts on the shear plane. The push-off test allows for the investigation of the shear behaviour and strength of the concrete interface, providing valuable insights into the load transfer mechanisms and structural performance under shear forces.

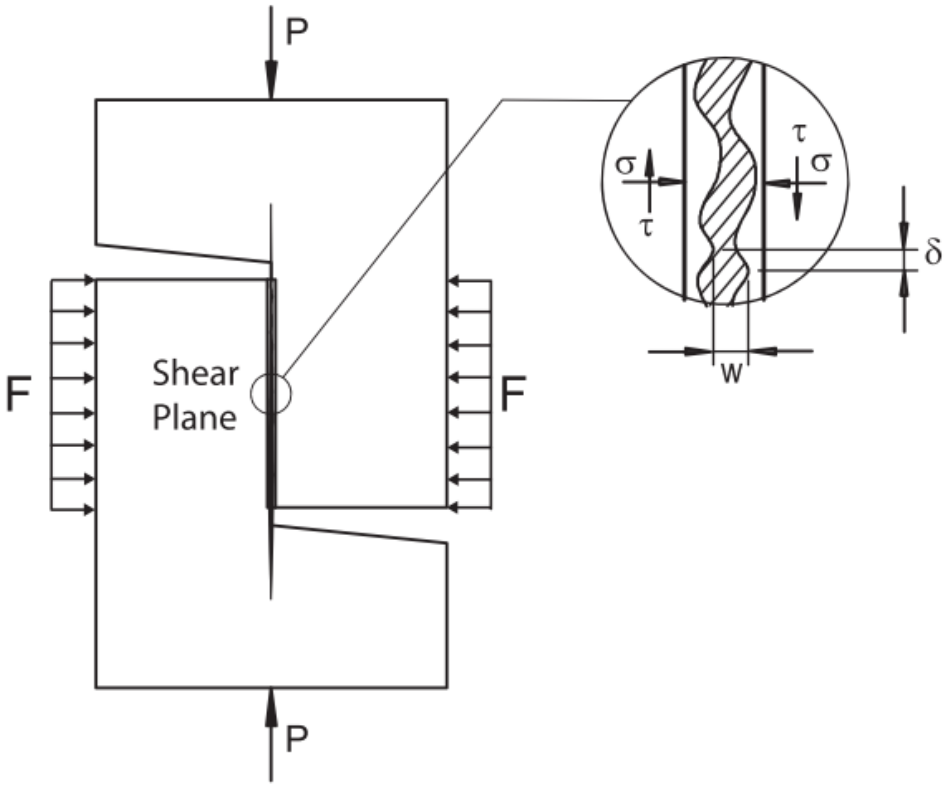



**Figure 2.6.** Displacements and stresses on the shear plane in push-off specimens (Echegaray-Oviedo et al., 2017)

## 2.3 Shear Retrofit Techniques

In recent years, the need for enhancing the shear capacity of existing RC structures has become a significant focus of research and practice in civil engineering. Shear retrofit in RC refers to the process of strengthening an existing concrete structure to improve its resistance to shear forces. Various techniques can be employed for shear retrofit in concrete structures, depending on the specific requirements and condition of the structure. One of the most common ways to improve the shear capacity of RC structural elements is to add near-surface mounted (NSM), or surface mounted, elements. This involves installing additional reinforcement, such as steel bars, plates, or fibre-reinforced polymers (FRPs), to enhance the shear capacity of the concrete element. The reinforcement is typically placed in strategic locations, such as near the supports or critical sections of the structure, where shear demands are known to be high. Another method to improve the shear response is the addition of concrete layers to the existing structure. Several highlights of these methods will be discussed in this section.

### 2.3.1 Addition of Steel Reinforcement

Steel elements can be bonded or bolted to an existing structural element to increase its strength and stiffness. Numerous experimental studies have demonstrated significant enhancement in the shear capacity of RC elements with the application of external steel reinforcement. Sharif et al. (1994) tested several arrangements of externally bonded steel plates on shear-deficient RC beams, obtaining shear strength increases for all the configurations and restoring stiffness. However, most of the specimens exhibited sudden failure due to plate separation.

Adhikary et al. (2000) conducted both numerical and experimental studies on enhancing the shear strength of RC beams. The study found that the addition of continuous horizontal steel plates externally with epoxy bonding had a positive impact on the ultimate shear strength of RC beams. This method also increased their flexural strength and stiffness. The construction process is simple, requiring minimal anchorage work, and proves to be an effective way of upgrading RC beams that need shear and flexural reinforcement. Additionally, the study found that the ultimate shear strength of a beam with web-bonded steel plates increased with greater plate depth and thickness along the beam section.

Altin et al. (2005) focused on investigating the strengthening of RC beams against shear using epoxy bonded steel plates with various arrangements (Figure 2.7). Successful bonding was closely linked to construction quality, such as surface roughening, thorough cleaning, and adherence to epoxy

application procedures. Experimental results revealed that all externally bonded steel member types improved beam strength, stiffness, and ductility. Strengthened specimens exhibited similar behaviour to the control specimen up to reaching yield strength with nearly the same stiffness. The type and arrangement of steel members influenced ductility behaviour and failure modes. Decreasing spacing between steel straps increased displacement ductility, while increasing bonding area on the shear span reduced shear crack propagation.

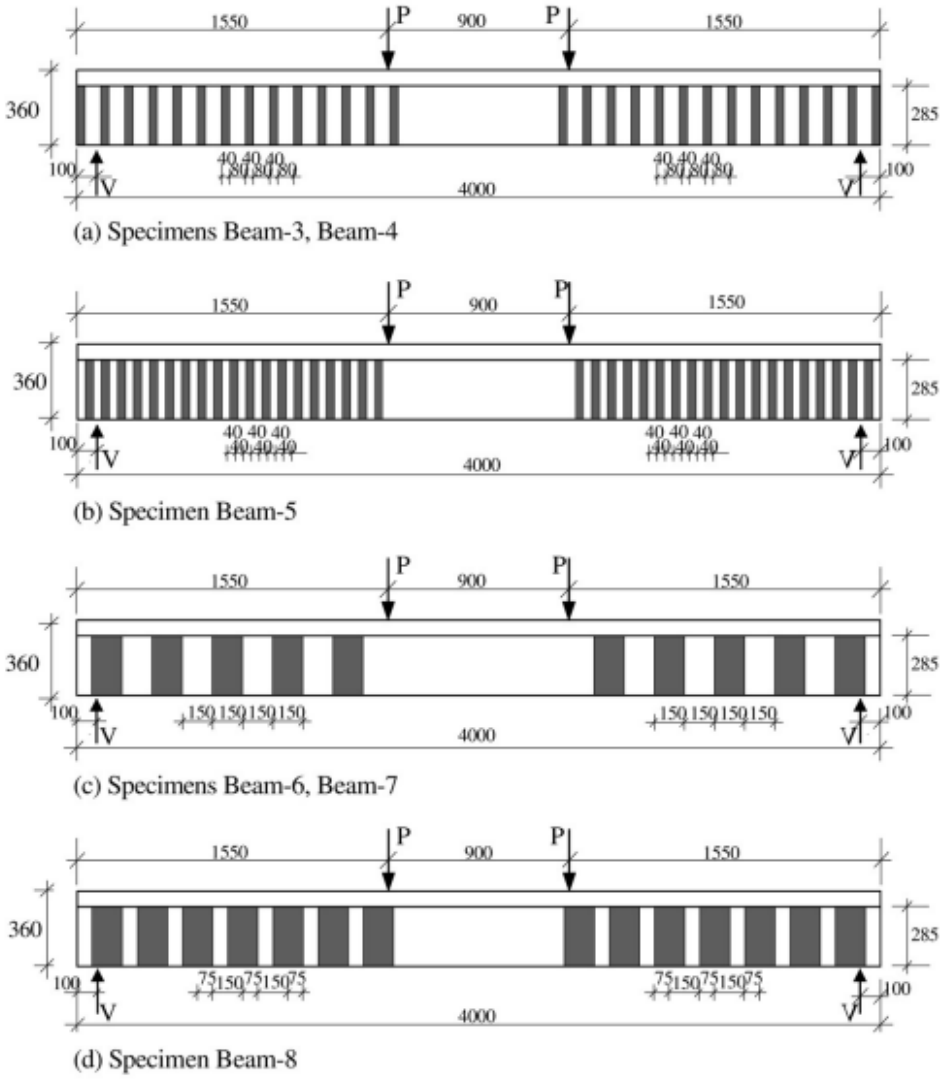



**Figure 2.7.** Steel strap and plate arrangements (Altin et al., 2005)

The use of external steel reinforcement for shear deficient RC beams provides notable benefits in terms of enhancing ultimate strength and ductility. However, certain disadvantages and gaps should be carefully considered. The technique is highly invasive, requiring extensive surface preparation and the use of large anchors, which may weaken the concrete and lead to structural modifications. Additionally, the long-term durability of the bonding interface needs thorough assessment, as exposure to environmental factors can compromise the effectiveness of the strengthening over time. Proper compatibility and design considerations are essential, and the structural integrity during retrofitting must be managed to prevent any adverse effects on the overall stability of the structure. Further, the addition of external skin reinforcement can also increase the flexural resistance of a member; thus, adding complications to retrofits that are aimed at preempting shear-governed failures.

In conclusion, while external steel reinforcement can significantly improve the shear capacity of deficient RC beams, careful evaluation and planning are necessary to address the potential challenges. Mitigating the invasiveness, ensuring long-term durability, and maintaining compatibility with existing concrete are crucial for successful implementation. Proper design and execution are essential to achieve optimal strengthening performance while minimizing negative impacts on the structure.

### 2.3.2 Addition of Fibre-Reinforced Polymer Strengthening

Another way to improve the shear capacity of RC structural elements that is gaining popularity rapidly in recent years is to use FRP strengthening. FRP is a composite material that consists of fibres, such as carbon or glass, embedded in a polymer matrix. FRP is lightweight, high strength, and corrosion-resistant, making it an attractive option for retrofitting existing RC structural elements. FRP strengthening can be used to increase the shear capacity of RC beams, columns, and slabs by wrapping the existing element with FRP. In recent years, numerous studies have been conducted to explore the effectiveness of FRP retrofits as shear strengthening solutions for RC structures. This section highlights key studies in the field.

Al-Mahmoud et al. (2015) explored the potential of using Carbon Fibre-Reinforced Polymer (CFRP) rods with the Near Surface Mounted (NSM) technique to enhance the shear strength of concrete structural members (Figure 2.8). Results demonstrated the effectiveness of NSM CFRP rods, providing significant shear strength improvements compared to beams reinforced solely with stirrups. The use of epoxy resin as a filling material outperformed mortar but with a moderate gain. The interface between

mortar and CFRP rods shows promising performance, while the cost-effectiveness of mortar makes it an attractive alternative.

De Lorenzis & Nanni (2001) aimed to explore the effectiveness of NSM FRP rods in enhancing flexural and shear strength of deficient RC members. Eight full-size beams, comprising two control beams and six strengthened beams, were tested to investigate variables such as rod spacing, strengthening pattern, end anchorage of rods, and the presence of internal steel shear reinforcement. Results confirmed that NSM FRP rods significantly increased the shear capacity of RC elements, with a potential capacity increase of up to 106 % observed in the absence of steel stirrups. Furthermore, even when internal shear reinforcement was below ACI requirements, the contribution of NSM rods remained substantial. Some observed failure modes involved debonding of FRP rods due to epoxy cover splitting, which could be mitigated by providing a larger bond length or using 45-degree rods at close spacing. However, this may shift the controlling factor to splitting of the concrete cover. The proposed model provided reasonably accurate predictions of shear capacity, though further research is needed to incorporate the influence of all significant variables into the formulae.

Rizzo & De Lorenzis (2009) conducted tests on beams strengthened with NSM reinforcement to analyze various parameters, including type, spacing, and inclination of the reinforcement, as well as the mechanical properties of the groove-filling epoxy. The results indicated that NSM FRP reinforcement significantly enhanced the shear capacity of RC beams, even in the presence of limited steel shear reinforcement. The NSM reinforcement was found to be more efficient in exploiting FRP tensile strength compared to externally bonded laminates. The failure mode for beams strengthened with NSM reinforcement was the separation of the side concrete covers of internal steel stirrups. The use of stiffer and stronger groove-filling epoxy and NSM strips instead of round bars resulted in a lower FRP contribution to shear capacity. Moreover, decreasing the spacing or increasing the inclination of bars did not benefit the shear capacity of the beam due to accelerated debonding failure patterns. The study highlighted the need for further research to understand all possible failure mechanisms and develop accurate predictive models for beams strengthened with NSM reinforcement.

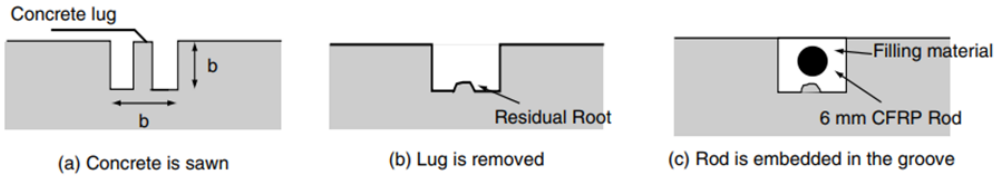



**Figure 2.8.** Installation of the NSM CFRP rod (Al-Mahmoud et al., 2015)

An experimental campaign conducted at The University of Texas (Jirsa et al., 2017; Shekarchi, 2016), explored the use of carbon fibre reinforced polymer (CFRP) strips on RC beams as a shear strengthening method (Figure 2.9). In a total of nine tests, the effectiveness of various parameters of large-scale RC pile cap girders was investigated. These factors included loading conditions, retrofitting of uncracked and cracked sections, placement of anchors in tension zones, and the use of uni- and bi-directional CFRP layouts. The results demonstrated that uni-directional CFRP layouts increased shear capacity by up to 56%, while bi-directional layouts enhanced the cracking shear load by up to 22%.

Notably, anchored CFRP layouts were as efficient as fully wrapped layouts despite anchor placement in tension zones. Additionally, the study highlighted that CFRP fracture strain values exceeded current design guidelines, prompting the development of rational design approaches and detailing recommendations for CFRP shear strengthening. Moreover, the study emphasized the importance of quality control procedures for CFRP installation, particularly for CFRP anchors, which currently lack established quality control measures. These findings contribute to the feasibility and effectiveness of CFRP strengthening techniques, especially for large bridge beams and girders, addressing the evolving demands of the Texas highway system and structural preservation.

Although FRP retrofitting offers numerous benefits, several challenges and research areas require attention. One significant challenge is the need for proper surface preparation and bonding to ensure effective transfer of shear forces between the FRP and concrete (Rizzo & De Lorenzis, 2009). Proper surface roughening and cleaning are critical to achieving a strong bond, and debonding failures must be carefully addressed in design and installation. Another aspect of concern is the effect of environmental exposure on FRP materials over time. Elevated temperatures, humidity, and exposure to ultraviolet (UV) radiation may cause degradation in the FRP, impacting its performance and long-term durability.



**Figure 2.9.** CFRP external reinforcement on wide-webbed RC beam (Shekarchi, 2016)

In summary, the use of FRP as a shear retrofit method in RC structures presents significant advantages, including high strength, durability, and lightweight properties. The non-invasive nature of FRP retrofitting makes it an attractive option for strengthening existing structures without compromising their original load-carrying capacity. However, challenges related to proper bonding, environmental exposure, and long-term performance necessitate thorough research and careful implementation. By addressing these challenges and advancing our understanding of FRP materials, this retrofitting technique can offer a reliable and effective solution to enhance the shear capacity and resilience of RC structures.

### 2.3.3 Concrete Jacketing

Concrete jacketing is a widely used rehabilitation technique for damaged or poorly detailed RC members. In this method, a new layer of concrete is added to the existing structure, involving the application of jackets around structural elements such as beams, columns, and joints. The jacketing process enhances the shear capacity and overall performance of RC structures, especially in earthquake-prone areas. Traditional concrete jackets and shotcrete overlays with external reinforcement have been commonly applied (Teran & Ruiz, 1992). However, it requires skilled labor, material compatibility, and careful quality control. Potential challenges include concrete shrinkage, cracking, higher costs, space constraints, and long-term durability considerations (Chalioris & Pourzitidis, 2012).

Chalioris & Pourzitidis (2012) conducted ten four-point bending loading tests on shear-damaged RC beams, with five of the beams retrofitted using reinforced U-formed self-compacting concrete (SCC) jackets (Figure 2.10). The main objective was to investigate the effectiveness of the SCC jacketing technique in restoring the shear-damaged beams. The results revealed that the SCC jacketing was an easy-to-apply and effective rehabilitation technique, fully restoring or enhancing the capacity of the retrofitted beams compared to the initial specimens. Retrofitted beams showed a significant increase in loading bearing capacity, ranging from 35 to 200 % compared to the initial beams. Moreover, the structural performance of most jacketed beams improved significantly, exhibiting enhanced ductile behaviour and pure flexural response, while initially tested beams demonstrated brittle shear response. Nevertheless, for one of the deep beams, questions arose about the ability of the SCC jacket to alter the brittle shear response to a more ductile one, warranting further research, especially for beams with larger cross-sectional dimensions.

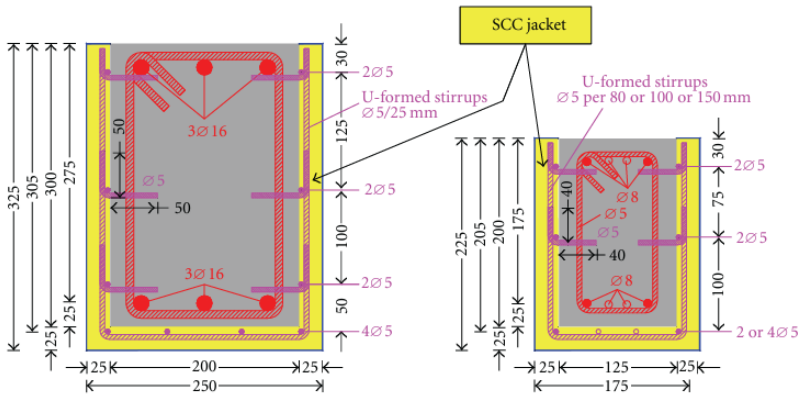



**Figure 2.10.** Jacketed beams (dimensions in mm) (Chalioris & Pourzitidis, 2012)

## 2.4 Shape Memory Alloys

### 2.4.1 Background:

Shape memory alloys (SMAs) are a class of metallic materials that undergo phase transformations under mechanical and thermal loading. These materials are known for displaying two unique thermomechanical properties: superelasticity and the shape memory effect. Superelasticity refers to the ability of the SMA to recover their original shape after having been subjected to large strains. The shape memory effect, on the other hand, allows SMAs to reverse plastic deformations and return to their original shape when heated.

SMAs were first discovered in 1932 by Arne Olander, a Swedish metallurgist, who found that a gold-cadmium alloy could "remember" its original shape after being deformed at low temperatures. The property was later observed in other alloys, including copper-zinc and copper-aluminum-nickel alloys, but the mechanism behind the effect was not fully understood (Ölander, 1932). It wasn't until the 1960s that the shape memory effect was fully understood. In 1962, William Buehler, a researcher at the Naval Ordnance Laboratory in White Oak, Maryland, discovered that a nickel-titanium alloy (NiTi) exhibited shape memory behaviour at room temperature (Buehler et al., 1962). Buehler's discovery paved the way for the development of practical SMAs, which are now widely used in a variety of applications.

The coming sections will introduce the main properties of SMAs, including their shape memory effect and superelasticity, as well as the martensitic phase transformation that governs these effects. The SMAs of interest for this study, iron-based SMAs will be introduced. Additionally, several

engineering applications of SMAs will be presented, highlighting their potential for improving the functionality and performance of diverse systems. Understanding the properties and behaviour of SMAs is critical for their successful integration into various engineering applications and can lead to the development of novel and innovative technologies.

### 2.4.2 Properties:

SMAs exhibit a unique ability to recover their shape after experiencing large deformations, achieved through either heating, known as the shape memory effect, or removal of load, known as the superelastic effect. This remarkable property is attributed to a martensitic phase transformation between the high-symmetry austenitic phase, characterized by a cubic crystal structure, and the low-symmetry martensitic phase, characterized by a monoclinic crystal structure (Desroches et al., 2004).

Figure 2.11 presents an illustrative stress-strain-temperature response for SMAs. The curves show three distinct phases of the SMA's behaviour (Zareie et al., 2020). The first phase is the elastic phase, in which the stress is directly proportional to the strain, and the SMA returns to its original shape when the stress is removed. The second phase is the transformation phase, in which the SMA undergoes a reversible change in its crystal structure, resulting in a change in its physical properties. During this phase, the stress remains relatively constant while the strain increases. The third phase is the plastic phase, in which the material undergoes permanent deformation and eventually fails. At low temperatures, the transformation phase is narrow, and the stress-strain curve remains relatively linear throughout the deformation process. As the temperature increases, the transformation phase becomes wider, and the stress-strain curve becomes more nonlinear. At high temperatures, the transformation phase disappears altogether, and the SMA behaves like a typical metal, with a linear stress-strain relationship in the elastic phase followed by plastic deformation and failure.

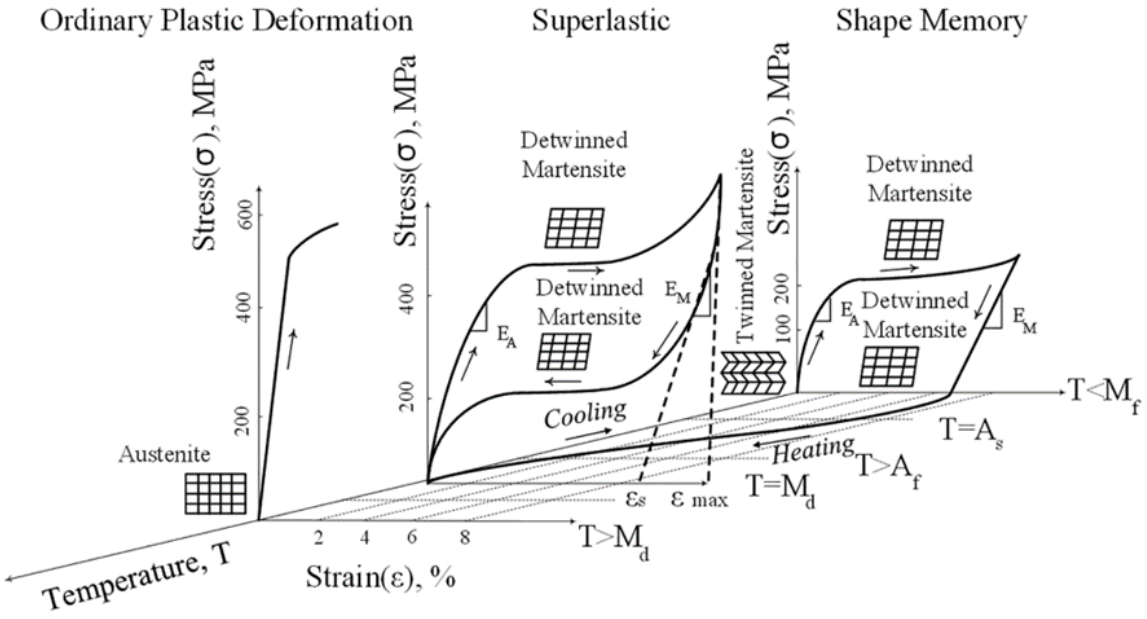



**Figure 2.11.** Stress-strain-temperature diagram of SMA adopted from (Zareie et al., 2020)

### 2.4.2.1 Austenite and martensite phases

SMAs exist in two phases: austenite and martensite. Austenite is the high-temperature phase, and martensite is the low-temperature phase. The shape memory effect is caused by a reversible transformation between these two phases. Austenite is the high-temperature phase of SMAs that possesses a face-centered cubic (FCC) crystal structure (Heo et al., 2009). In this phase, the atoms are arranged in a regular pattern and the material is relatively soft and ductile. Austenite is stable at high temperatures and can be deformed easily,

Martensite, on the other hand, is the low-temperature phase of SMAs that has a body-centered tetragonal (BCT) or a body-centered cubic (BCC) crystal structure. This phase forms when austenite is cooled rapidly, such as by quenching. Martensite is harder and more brittle than austenite, and it exhibits a unique lattice distortion that gives it the ability to undergo large reversible deformation (Guo et al., 2007).

The reversible phase transformation between austenite and martensite phases is driven by temperature and stress. There are four main transformation temperatures in SMAs: Martensite start temperature ($M_s$), Martensite finish temperature ($M_f$), Austenite start temperature ($A_s$), and Austenite finish temperature ($A_f$). The transformation temperatures are dependent on the composition and

processing of the SMA. The Martensite start temperature ($M_s$) is the temperature at which the alloy starts to transform from its high-temperature austenitic phase into its low-temperature martensitic phase upon cooling. The Martensite finish temperature ($M_f$) is the temperature at which the transformation from austenite to martensite is complete upon cooling. The Austenite start temperature ($A_s$) is the temperature at which the alloy starts to transform from its low-temperature martensitic phase back to its high-temperature austenitic phase upon heating. The Austenite finish temperature ($A_f$) is the temperature at which the transformation from martensite to austenite is complete upon heating. The temperature beyond which stress-induced martensite can no longer occur is known as $M_d$ (Ma et al., 2010). At higher temperatures, the SMA behaves like any other regular metallic material and becomes permanently deformed. The transformation temperatures are crucial in determining the functional properties of SMAs, such as shape memory effect and superelasticity. By controlling the transformation temperatures through various methods such as alloying and heat treatment, the functional properties of SMAs can be tailored for specific applications.

#### 2.4.2.2 Superelasticity:

Superelasticity, also known as pseudoelasticity, refers to the ability of SMAs to recover their original shape even after being subjected to large amounts of strain, without undergoing permanent deformation. This property is due to the material's ability to undergo a reversible martensitic transformation, which allows it to store and release large amounts of elastic energy (Otsuka & Shimizu, 1986).

#### 2.4.2.3 Shape memory effect:

The shape memory effect is the ability of SMAs to recover their original shape after being deformed when heated above a certain temperature. This property is due to the material's ability to undergo a reversible austenitic transformation, which allows it to "remember" its original shape and recover it upon heating. The shape memory effect originates from the martensitic transformation that occurs when the alloy is cooled from a high-temperature austenite phase (Mohd Jani et al., 2013; Otsuka & Shimizu, 1986)

### 2.4.3 Composition and Commercially Available SMAs:

Shape memory alloys (SMAs) are available in several types commercially. The most widely used SMA is Nitinol (Nickel-Titanium), which finds application in medical devices like stents and dental braces. Copper-based alloys are popular in automotive and aerospace industries for their resistance to fatigue

and high temperature stability. Iron-based alloys are used for structural applications, actuators and sensors. Gold-cadmium, a unique SMA, can change shape in response to light, making it ideal for optical applications. Another unique SMA, silver-cadmium, changes shape in response to heat or electrical current, making it useful in various applications like switches and sensors. Other SMAs include nickel-manganese, nickel-aluminum, and copper-zinc-aluminum among others, which have specific properties that make them suitable for specific applications (Mohd Jani et al., 2013).

Among the most widely available Shape Memory Alloys (SMAs) on the market, Nickel-Titanium (NiTi or Nitinol) stands out as a prominent and extensively studied material. Research investigations have explored the potential use of NiTi SMAs for prestressing and active confinement purposes (El-Tawil & Ortega-Rosales, 2004; Shin & Andrawes, 2010). Nitinol exhibits a unique combination of superelasticity and shape memory effect properties, making it a versatile choice for various engineering applications, including medical devices, aerospace components, and robotics. The adoption of NiTi in structural applications has faced certain limitations primarily due to its relatively high cost, which has prevented its broader adoption.

#### 2.4.3.1 Iron-based shape memory alloys:

Iron-Based Shape Memory Alloys (Fe-SMAs) present a promising alternative to NiTi alloys in structural applications. Fe-SMAs use low-cost raw materials and can be easily produced under atmospheric conditions (Cladera et al., 2014). Fe-SMAs exhibit remarkable mechanical properties, including high tensile strength and an impressive shape memory effect. These alloys can be easily manufactured into various shapes, such as wires, strips, and plates, both in hot and cold conditions, without compromising their ductility or strength (Czaderski et al., 2015; K. Hong et al., 2018). Fe-SMAs are known for their durability, requiring low maintenance, and offering corrosion resistance similar to stainless steel (Zhang et al., 2022). When subjected to pre-straining, restraining, and heating to an activation temperature of about 200ºC, Fe-SMAs display the ability to self-prestress (Figure 2.12), generating high recovery stresses exceeding 300 MPa (Jeong et al., 2022). This shape memory effect enables the active confinement of structural elements and the potential reduction of existing cracks when appropriately restrained (Czaderski et al., 2015; K. Hong et al., 2018). An intriguing advantage of Fe-SMAs is their capacity for self-prestressing, eliminating the need for hydraulic or jacking equipment; instead, resistive energy is sufficient for prestressing the alloy (Rojob & El-Hacha, 2018).

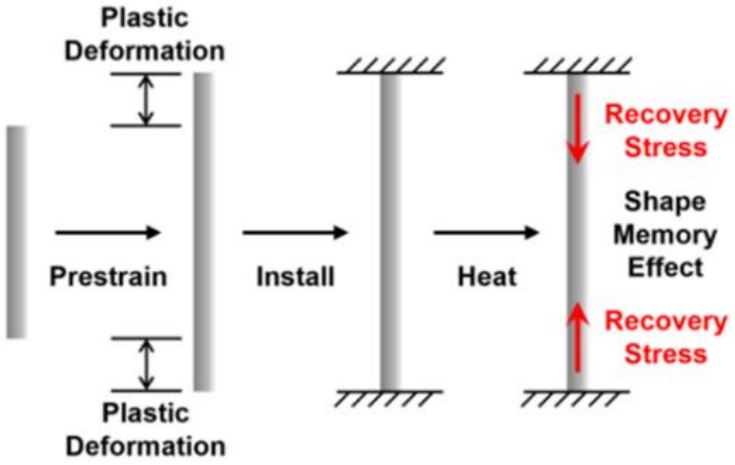



**Figure 2.12.** Fe-SMA prestressing concept (González-Góez et al., 2023)

Fe-SMAs exhibit considerable potential not only in material prestress strengthening but also in the dissipation of energy from low cycle fatigue loads, owing to their steady hysteric behaviour (Zhang et al., 2022). As highlighted by Rosa et al. (2021), Fe-SMAs possess the capacity to store substantial elastic strain energies and demonstrate superior plastic stiffness and ductility compared to conventional steel, making them a highly attractive material for seismic applications. One of the key characteristics of Fe-SMAs under cyclic loading is the occurrence of phase transformation between austenite and a tension and compression-induced martensite. This phase transformation plays a crucial role in reducing the concentration of internal stresses and local dislocations, thereby effectively preventing fatigue cracking behaviour (Zhang et al., 2022).

However, it is essential to acknowledge that Fe-SMAs may exhibit a loss in recovery stress ranging from 10 to 20 % under strain ranges of 0.035 and 0.07 %. This consideration becomes crucial during the design phase to ensure the optimal performance of the alloy in structural applications (Ghafoori et al., 2017). Despite this limitation, the promising attributes of Fe-SMAs, such as their energy dissipation capabilities and resistance to fatigue cracking, make them a compelling alternative for various engineering applications, including seismic-resistant structures and fatigue-sensitive systems. As research into Fe-SMAs continues to advance, their full potential in enhancing the durability and performance of structural components will likely be further realized, opening new possibilities in the field of engineering materials and design.

### 2.4.4 Fe-SMA Applications in RC Structures:

Significant attention has been devoted to the advantages of Fe-SMA in RC structures. Wang & Zhu (2022) evaluated the cyclic behaviour of Fe-Mn-Si-based SMA bars with a buckling restrained brace (BRB) through cyclic tension-compression loading tests. The cyclic properties such as hysteretic response, recovery capability, fatigue behaviour, and fracture behaviour were evaluated with varying strain amplitudes and different loading patterns and the results showed that the Fe-SMA bars displayed satisfactory and stable hysteretic loops with excellent energy dissipation and symmetric behaviour under cyclic tension-compression loadings.

Several studies have also explored the flexural improvements of Fe-SMA retrofits. Shahverdi et al. (2016) investigated the use of low-cost Fe-SMAs as a cost-effective alternative for NSM strengthening of RC beams (Figure 2.13). Fe-SMA strips were utilized as prestressing elements in the beams, and the feasibility of this strengthening technique was demonstrated experimentally. The results showed that the beams strengthened with prestressed Fe-SMA strips exhibited significantly higher cracking loads and lower mid-span deflections compared to non-prestressed Fe-SMA-strengthened beams. Prestressing with Fe-SMAs offered various advantages, including reduced crack widths, deflections, and internal steel stress. Fe-SMAs were found to be easier to prestress than CFRP strips, as they do not require mechanical jacks or anchor heads. The bond behaviour of ribbed Fe-SMAs with cement-based mortar were satisfactory, and recovery stresses after activation reached approximately 200 MPa. Overall, the study successfully demonstrated the application of Fe-SMAs for strengthening and prestressing RC beams.

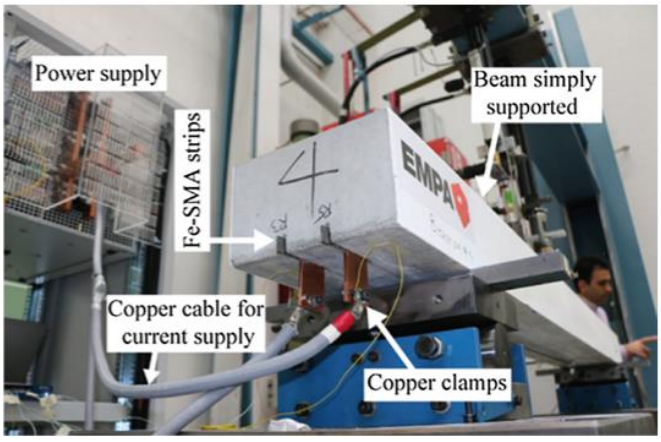



**Figure 2.13.** RC beam strengthened with NSM Fe-SMA strips (Shahverdi et al., 2016)

Schranz et al. (2021) aimed to explore innovative and effective strengthening methods for concrete members using Fe-SMA reinforcements in RC slabs (Figure 2.14). Two prestressed strengthening techniques were investigated: one involving the removal of concrete cover and installation of Fe-SMA bars with an additional mortar layer, and the other using grooves in the concrete cover for NSM Fe-SMA bars with mortar. Prestressing was achieved through resistive heating of the Fe-SMA bars. The strengthened specimens exhibited significant improvements in cracking, yielding, and ductility without premature failure of the strengthening reinforcement. The prestressing process was successful, and the surrounding cementitious material remained functional during loading. Longitudinal cracks were observed in the cover, but their width was negligible compared to current standards. Various analytical approaches were used to estimate the prestress, which confirmed the effectiveness of the prestressing procedures. The proposed strengthening methods involving Fe-SMA reinforcement have considerable potential for practical onsite applications due to their short installation time and simple prestressing process.

Soroushian et al. (2001) first demonstrated the potential for Fe-SMA shear strengthening by using externally mounted Fe-SMA rods to restore the load carrying capacity of a shear damaged RC beam. Fe-SMA rods (Figure 2.15) were used to generate significant recoverable strains when heated above a transformation temperature. The process involved pre-elongating shape memory rods at ambient temperature, anchoring them to the structural system, and then applying corrective forces through electrical resistance heating. The laboratory and field tests demonstrated the effectiveness of this approach in repairing flexural and shear damage in RC beams. The recoverable strains of shape memory rods were found to be relatively large compared to traditional steel and composites, reducing losses of prestressing force caused by factors such as anchorage slippage. In the subsequent section, an overview of additional studies concerning shear strengthening with Fe-SMA.



**Figure 2.14.** Fe-SMA strengthened RC slab (Schranz et al., 2021)

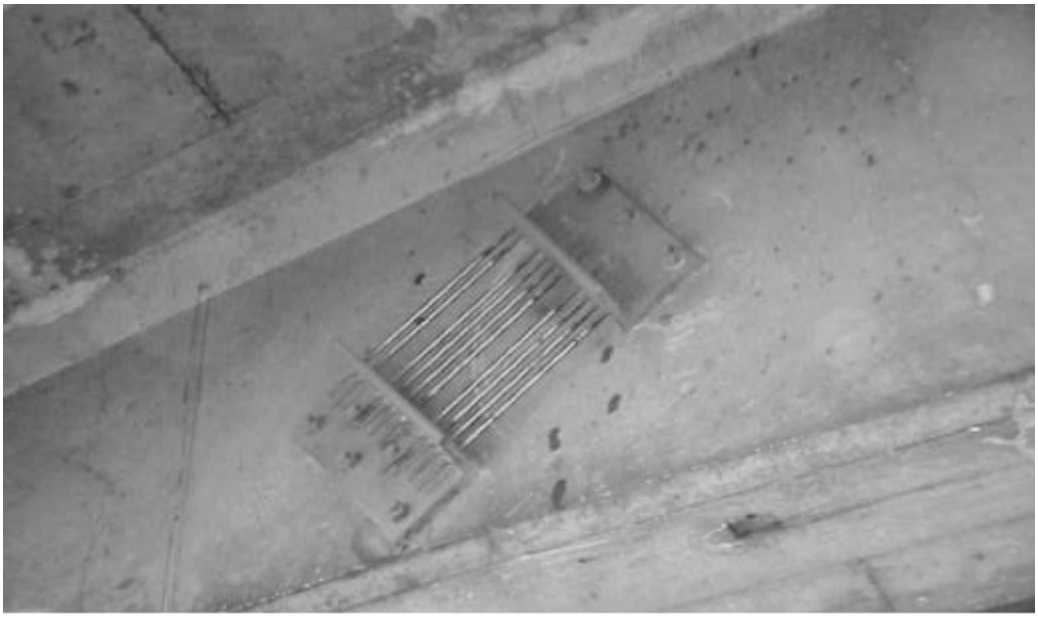


**Figure 2.15.** Fe-SMA rods for enhancement of shear resistance (Soroushian et al., 2001)

## 2.5 Fe-SMA Shear Strengthening

The use of SMAs as retrofit for shear-damaged concrete structures has gained significant attention in recent years. Several experiments have been conducted with addition of external Fe-SMA transverse reinforcement in Spain and Switzerland. Cladera et al. (2020) presented an experimental campaign involving real-scale RC beams. These beams had T-shaped cross-sections and were externally strengthened using U-shaped Fe-SMA strips (Figure 2.16). The tests revealed that the retrofitted beams exhibited approximately 30 % greater shear strength compared to the reference beams, and their flexural capacities were nearly achieved. The active strengthening approach proved effective in delaying crack formation and reducing their widths under service loads. However, it was observed that the U-configuration used for the strips required anchoring them to the web, possibly weakening the flange-web connection and hindering the proper transfer of tensile stresses between the longitudinal tensile reinforcement and the compression flange. As a result, the retrofitted beams showed less ductile behaviour than expected. All the beams ultimately failed in shear, and the retrofitting process enhanced the shear strength by about 30 %. The U-configuration for the strips, however, posed challenges in terms of strengthening efficiency and prediction accuracy.

Czaderski et al. (2021) developed a shear retrofit method using externally installed Fe-SMA stirrups in combination with a sprayed mortar (Figure 2.17). Large-scale experiments on T-beams confirmed the practicality and efficiency of the memory-steel shear strengthening. The technique showed promising results, significantly increasing shear capacity, and reducing beam deflections, internal steel stirrup stresses, and the number and width of cracks. Some key aspects highlighted in the study include the successful on-site application of the U-shaped ribbed bars, the effectiveness of the strengthening system in increasing load-bearing capacity, and the ability of prestressed memory-steel stirrups to delay shear crack appearance and reduce crack widths and mid-span displacements. Moreover, prestressing the memory-steel stirrups proved beneficial in reducing stress levels in internal steel stirrups, making it particularly suitable for infrastructure elements likely to experience cyclic/fatigue loading. The investigation demonstrated that the method was capable of repairing heavily-damaged RC beams, showcasing the potential of Fe-SMA for shear strengthening of concrete girders.

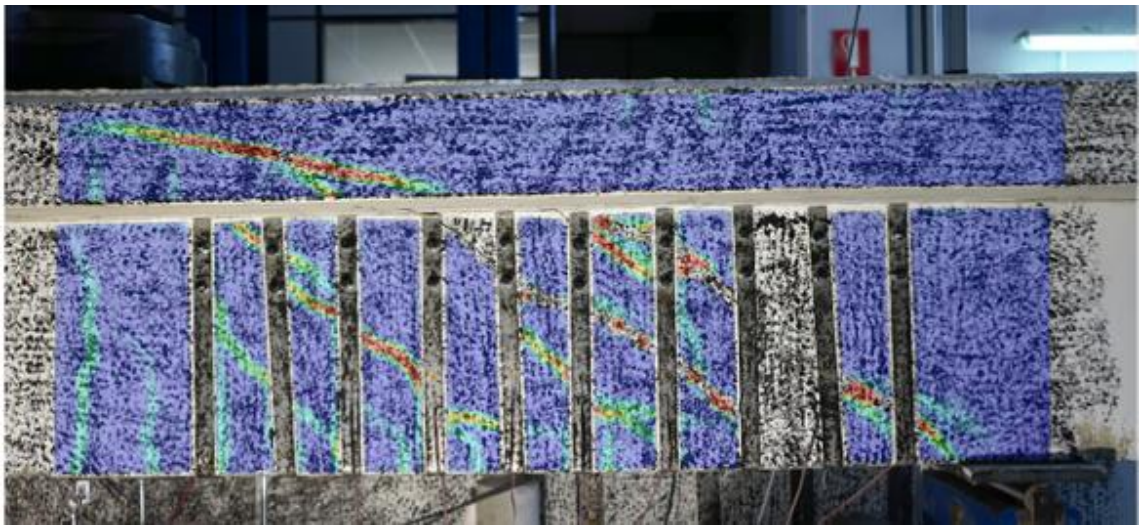


**Figure 2.16.** Fe-SMA strengthened beam (Cladera et al., 2020)



(a) Installed Fe-SMA stirrups. (b) Application of spray mortar

**Figure 2.17.** Fe-SMA shear strengthening with spray mortar (Czaderski et al., 2021)

Researchers at the University of Balearic Islands (Montoya-Coronado et al., 2019; Rius et al., 2019) evaluated the possibility of strengthening shear-critical beams with Fe-SMA strips (Figure 2.18) and their results showed a promising performance of the proposed technology, with an increase in both the shear strength of the retrofitted beams and their deflection at failure. An increase in shear strength of 92 % was achieved for the strengthened beams compared to non-strengthened beams.

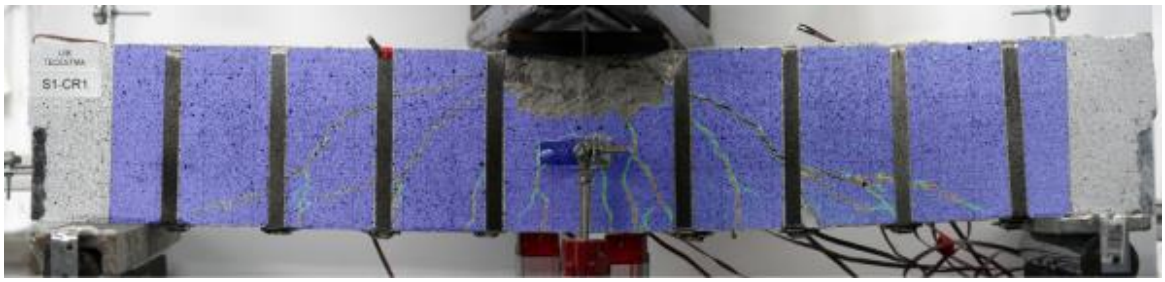



**Figure 2.18.** Beam with activated Fe-SMA strips (Montoya-Coronado et al., 2019)

To further optimize the proposed technology, additional research on real-scale elements is recommended, particularly to explore the enhancement of ductility using alternative anchorage systems or a full wrapping method by anchoring strips to the compression chord. This investigation will shed light on the potential efficiency improvements and contribute to a comprehensive understanding of the technology's applicability in practical engineering scenarios.

## 2.6 Summary

This chapter provides a comprehensive examination of shear strengthening techniques for concrete structures, with a particular emphasis on the application of Fe-SMAs. It begins with a general overview of the behaviour of concrete under shear, covering aspects such as shear damage, shear design and analysis models, and push-off testing. Then, various shear retrofit techniques are explored, including the addition of steel reinforcement, FRP strengthening, and concrete jacketing.

The review then shifts its focus to SMAs, presenting a detailed analysis of their properties, composition, and commercial availability. Notably, it highlights the potential of Fe-SMAs in concrete structures, discussing their diverse applications. Subsequently, the review explores Fe-SMAs specifically as a shear strengthening method, examining their feasibility and effectiveness. In conclusion, the literature review offers valuable insights into the use of Fe-SMAs, and other shear retrofit techniques, laying the foundation for further investigation and application in concrete structures.

# Chapter 3
# Finite Element Modelling

## 3.1 General

The objective of this chapter is to numerically examine the effectiveness of Fe-SMA as an active strengthening method for shear-damaged RC beams. An experimental specimen presented in the literature and involving a full-scale conventional RC pier cap element was modelled using the nonlinear finite element analysis (NLFEA) software program VecTor2 (Wong et al., 2013). Prestressed Fe-SMA elements were introduced in the model to simulate the addition of transverse reinforcement strengthening and a parametric analysis was performed to investigate the influence of various SMA reinforcement parameters that are expected to play key roles on strengthened component shear resisting performance:

i) the Fe-SMA reinforcement ratio,

ii) the level of SMA prestressing,

iii) the orientation of the simulated SMA retrofit, and

iv) the presence of conventional internal transverse reinforcement (i.e., steel stirrups).

The findings of this chapter will provide insight, generated by way of numerical modelling, into the shear resisting performance of RC components employing novel active shear-strengthening techniques and also illustrate cost-effective modelling strategies that can be utilized to investigate other, or similar, shear retrofits.

## 3.2 Preliminary Validation and Benchmark Analysis

VecTor2 (Wong et al., 2013) is a RC-dedicated NLFEA program. Cracked concrete material modelling is based on the on the formulations of the Disturbed Stress Field Model (DSFM) (Vecchio, 2000), which is an extension of the Modified Compression Field Theory (MCFT) (Vecchio & Collins, 1986). The program is suitable for the analysis of two-dimensional RC membrane structures subjected to quasi-static or dynamic loading. A total load, secant stiffness-based, solution procedure is used and provides stable solutions for all stages of response, making VecTor2 particularly appealing for the analysis of shear-sensitive structures that tend to exhibit abrupt changes in material stiffness and

response, and are often governed by highly brittle failure mechanisms. Second-order effects and other concrete and reinforcement related mechanisms that are not inherently accounted for in the formulations of the DSFM (e.g., concrete confinement and dilatation, plain concrete tension softening, concrete and steel hysteretic responses, etc.) are considered in the analysis, making the program suitable for a broad range of RC elements and analysis scenarios. In this chapter, NLFEA of large-scale beam-type elements are carried-out using VecTor2. The geometry and reinforcement details of the beams are based on those from the testing program reported in Jirsa et al. (2017) and Shekarchi (2016), which entailed the testing of RC bridge pier cap girders strengthened with CFRP shear retrofits. In the present study, an experimental control test specimen referred to as D-U-VN-HN* was used as a benchmark for assessing relative performance of Fe-SMA shear retrofitted components and also for validating the overall suitability of the finite element meshing, material models employed, and analysis strategy.

An illustration showing the control beam geometry and reinforcement detailing is presented in Figure 3.1. The beam was constructed with a square cross section measuring 813 by 813 mm, and a total length of roughly 8.4 m. The beam was designed such that the test span region (see Figure 3.1) would govern the capacity of the member and would be controlled by shear failure mechanisms. Two-legged 16-mm diameter stirrups were placed at a spacing of 457 mm, resulting in a shear reinforcement ratio of 0.11 % within the test span, which is on the order of recommended minimum shear reinforcement requirements in modern North American provisions (AASHTO LFRD 2019, CSA A23.3:19). 11 US No. 11 bars were provided as longitudinal flexural reinforcement on both the tension and compression sides of the cross section resulting in a flexural tension and compression reinforcement ratio of 1.9 %. The beam was tested using a skew-symmetric loading configuration that produced an inflection point at the midspan of the test span region, thus resulting in a double-curvature bending scenario. Additional details regarding the beam geometry and reinforcement, and the testing procedure used in the experimental program, are available in Jirsa et al. (2017).

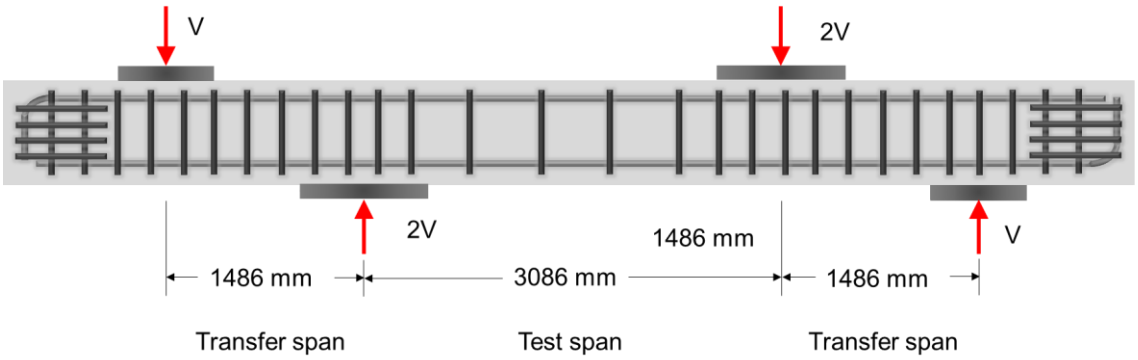



**Figure 3.1.** Jirsa et al. (2017) double-curvature control beam.

### 3.2.1 Modelling Approach

Figure 3.2 presents the two-dimensional finite element mesh developed for the Jirsa et al. (2017) RC control beam. In total, the finite element mesh consisted of 1,266 rectangular finite elements that were used to represent different RC material types, steel bearing plates, and load/support interface regions. Flexural longitudinal reinforcement was modelled explicitly using 408 truss bar finite elements that were assumed to be perfectly bonded with the surrounding concrete. All transverse reinforcement was modelled in a smeared sense, using different RC material types to represent the different transverse reinforcement ratios provided over the length of the beam. The analysis was performed in a displacement- controlled manner, with equal and opposite displacements applied at the interior load bearing locations, and a roller and pin support reaction were provided at the two exterior bearing locations. Note that self-weight of the RC beam was neglected.

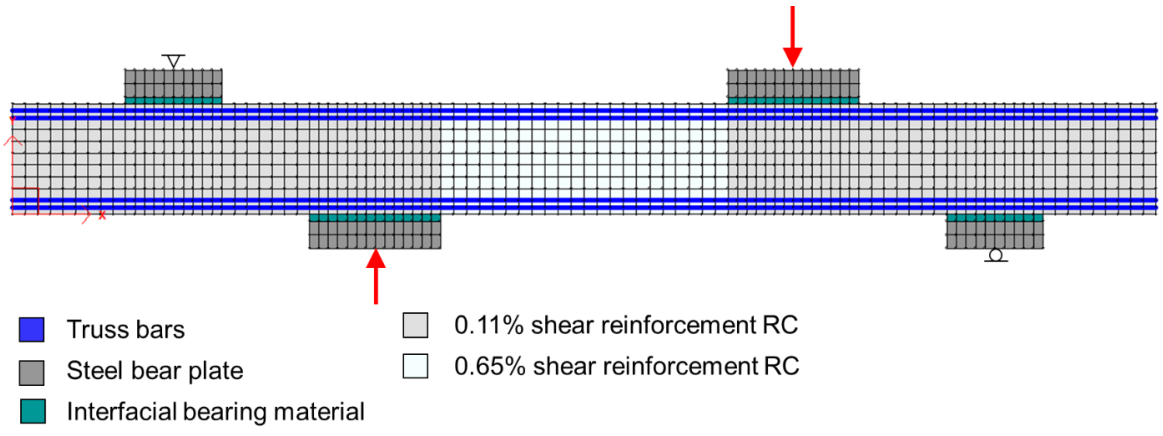
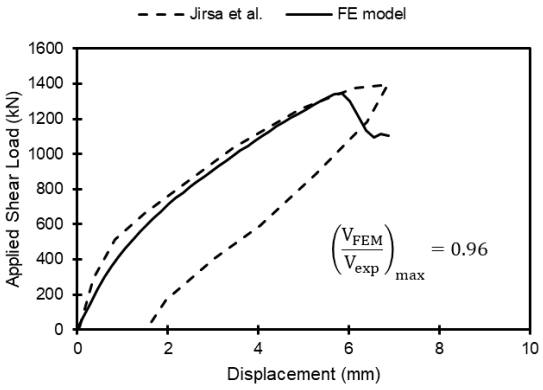



**Figure 3.2.** VecTor2 two-dimensional model

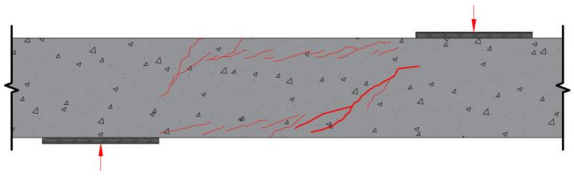
All user-definable material models and analysis parameters corresponded with VecTor2's default modelling options. More specifically, no effort was made to parametrically define models or refine analysis results, and user input was limited to the definition of the concrete and steel reinforcement materials properties, which were specified to match those reported in Jirsa et al. (2017). For reference, the concrete material was defined with a cylinder strength of 31 MPa and a maximum nominal aggregate size of 25 mm. Flexural reinforcement was assigned a yield strength of 420 MPa and a modulus of elasticity of 200,000 MPa. Shear reinforcement was assigned a yield strength of 400 MPa and a modulus of elasticity of 200,000 MPa.

### 3.2.2 Validation for Benchmark RC Beam

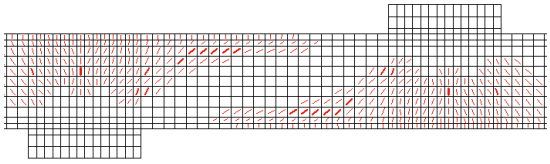
To validate the effectiveness of the meshing and behavioural models employed, results in the form of applied shear versus loading point displacement are presented in Figure 3.3 and compared to the reported experimental data. From the figure, the shear capacity is estimated within 5 % of that reported. Further, it can be seen that the finite element model developed was generally capable of capturing all aspects of the reported response ranging from the post-cracking shear stiffness, the capacity of the RC beam, and the brittle shear-governed failure mode encountered.




(a) computed shear force-displacement response



(a) reported damage at ultimate (Jirsa et al., 2017)



(c) computed damage at ultimate (VecTor2)

**Figure 3.3.** Results for Jirsa et al. (2017) RC Control Beam.

## 3.3 Parametric Study

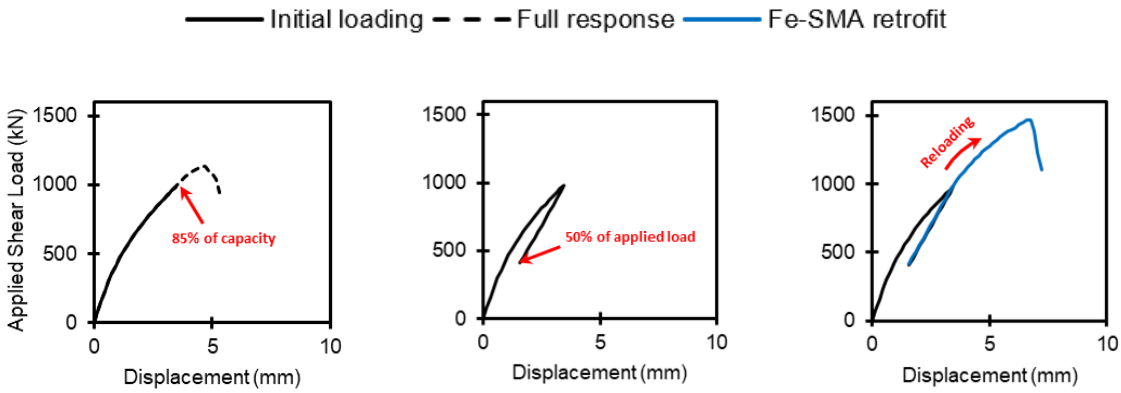
In this section, a parametric study used to investigate the impacts of introducing externally bonded Fe-SMA retrofit to shear-damaged RC beams is presented. The geometry is based on the pier cap test beam described in Section 3.2. Parameters selected for investigation include the amount of transverse Fe-SMA reinforcement in the test span, the level of Fe-SMA prestressing, the presence of existing internal transverse reinforcement, and addition of longitudinally oriented Fe-SMA within the web region of the beam and in the amount of 0.10 %. Table 3.1 summarizes the parameters considered in the study.

**Table 3.1.** Summary of parameters.

| Prestress level (MPa) | Fe-SMA Reinf. Ratio (%) | Fe-SMA Direction | Existing Shear Reinf. Ratio |
|---|---|---|---|
| 266 | 0.10 | Vertical only | No. Reinf. |
| 399 | 0.20 | Vertical + Horizontal | Min = 0.083%* |
| | 0.30 | | |
| | 0.40 | | |

*Computed according to Clause 11.2.8.1, (CSA A23.3:19)

To simulate the presence of initial shear damage that would prompt the need for shear retrofitting, and to subsequently estimate the effectiveness of the different Fe-SMA retrofits, the NLFEA was performed in three phases: 1) *initial loading*: a seed model of the RC beam was first loaded up to approximately 85 % of the peak capacity to induce shear damage/distress in the RC component (see Figure 3.4a), 2) *unloading*: the beam was then unloaded to 50 % of the initially-applied load (see Figure 3.4a), 3) *retrofit and reloading*: at this point, prestressed Fe-SMA reinforcement was added within the previously defined test span region (see Figure 3.1) as smeared reinforcement and the analysis was resumed until failure was estimated to occur (see Figure 3.4c). Figure 3.4 presents a schematic view of the 3-phase progression of analyses performed.




(a) initial loading (b) unloading (c) retrofit and reloading

**Figure 3.4.** NLFEA loading phases.

The Fe-SMA was added to the model as smeared reinforcement in the test span of the beam (see highlighted region in Figure 3.5. Shape Memory Alloy (type 2) material from the VecTor2 library was used to define the constitutive models governing the response of the Fe-SMA retrofit and its associated material properties were defined to match those reported by Hong et al. (2018) (yielding stress = 463 MPa, ultimate tensile strength = 863 MPa and modulus of elasticity = 133,000 MPa). The Fe-SMA behaviour is shown in Figure 3.6.

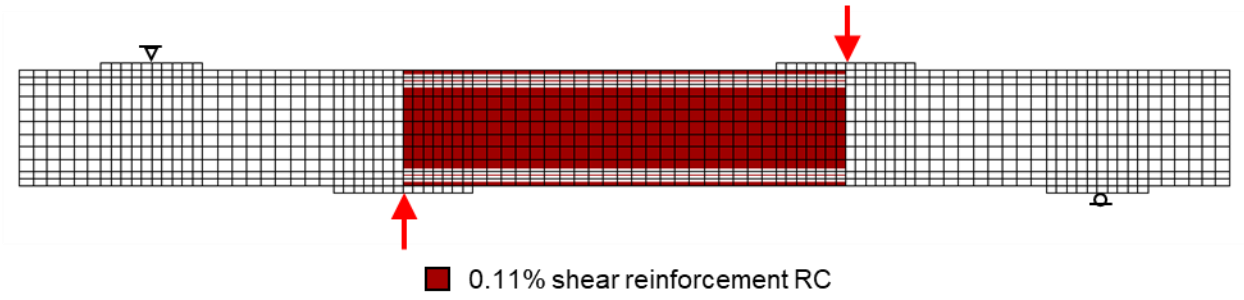



**Figure 3.5.** VecTor2 mesh with smeared Fe-SMA retrofit.

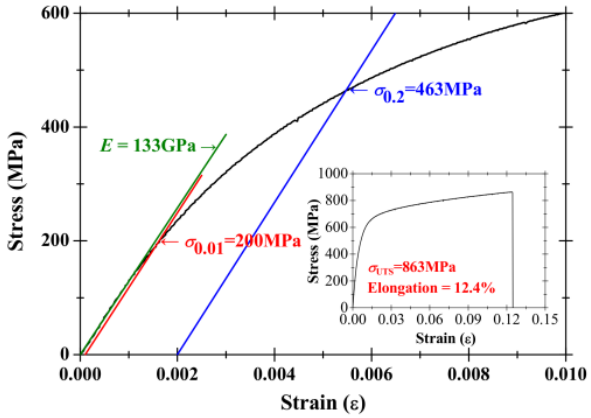



**Figure 3.6.** Fe-SMA stress-strain response (K. Hong et al., 2018)

## 3.4 Results and Discussion

The analyses were performed using four different finite element seed models to represent the varying levels of internal transverse reinforcement and the different directions/orientations of external Fe-SMA reinforcement. The seed models were denoted as VN, VT, BDN and BDT where V = vertical Fe-SMA, BD = bidirectional Fe-SMA, N = No transverse reinforcement, and T = minimum transverse reinforcement.

### 3.4.1 Shear Response

Figure 3.7 presents the applied shear versus displacement results before and after Fe-SMA retrofits were incorporated into the models. It can be observed that as the external shear reinforcement ratio ($\rho_v$) is increased, shear capacity and displacement at peak shear resistance increased. A slight increase is also obtained by way of the transverse prestressing applied via the Fe-SMA; however, when contrasted with the impact of shear reinforcement ratio, increase the level of Fe-SMA prestressing from 286 to 399 MPa is estimated to be less significant to shear capacity. The post-retrofit stiffness was found to follow the unloading curve of the seed models and exhibited only marginal softening after reaching and exceeding previous load levels. Results pertaining to shear capacity and corresponding shear strength gains compared to seed model analyses without any form of shear retrofit, are summarized in Table 3.2. Maximum estimated shear strengths were 1135 kN for the models without internal transverse reinforcement (VN, BDN) and 1293 kN for models with transverse reinforcement (VT, BDT).

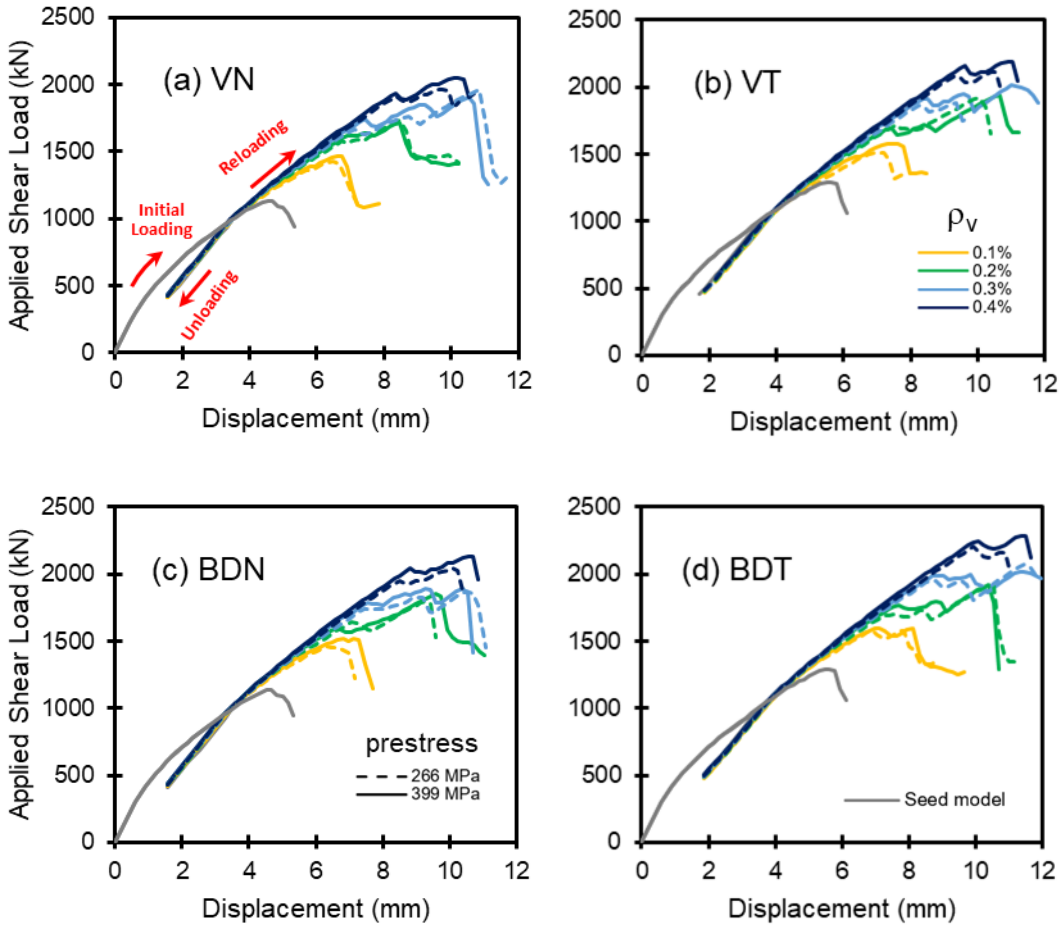



**Figure 3.7.** Shear response

**Table 3.2.** Peak shear capacities and retrofit strength gains

| Seed model | Prestressing level (MPa) | Fe-SMA reinforcement ratio | | | | | | | |
|---|---|---|---|---|---|---|---|---|---|
| | | 0.1% | 0.2% | 0.3% | 0.4% | 0.1% | 0.2% | 0.3% | 0.4% |
| | | Peak shear (kN) | | | | Peak shear increase (%) | | | |
| VN | 266 | 1429 | 1736 | 1962 | 2102 | 26 | 53 | 73 | 85 |
| | 399 | 1466 | 1716 | 1908 | 2013 | 29 | 51 | 68 | 77 |
| VT | 266 | 1509 | 1924 | 2012 | 2169 | 17 | 49 | 56 | 68 |
| | 399 | 1581 | 1943 | 2012 | 2190 | 22 | 50 | 56 | 69 |
| BDN | 266 | 1459 | 1800 | 1873 | 2078 | 29 | 59 | 65 | 83 |
| | 399 | 1516 | 1849 | 1893 | 2134 | 34 | 63 | 67 | 88 |
| BDT | 266 | 1583 | 1910 | 2070 | 2204 | 22 | 48 | 60 | 70 |
| | 399 | 1601 | 1919 | 2018 | 2285 | 24 | 48 | 56 | 77 |

Additional models were developed to further investigate the impact of different shear reinforcement prestressing levels on the shear response of the beam. Figure 3.8 presents computed shear force - displacement responses for the VN seed model with a Fe-SMA shear retrofit of 0.10 % and Table 3 summarizes the shear capacities obtained for the different retrofits. Five different Fe-SMA prestressing levels were considered: zero, 133 MPa, 266 MPa, 333 MPa, and 399 MPa. From the data presented, it can be seen that the prestressing level does indeed enhance the shear resisting performance of the beam by way of delaying stiffness degradation and by increasing shear capacity.

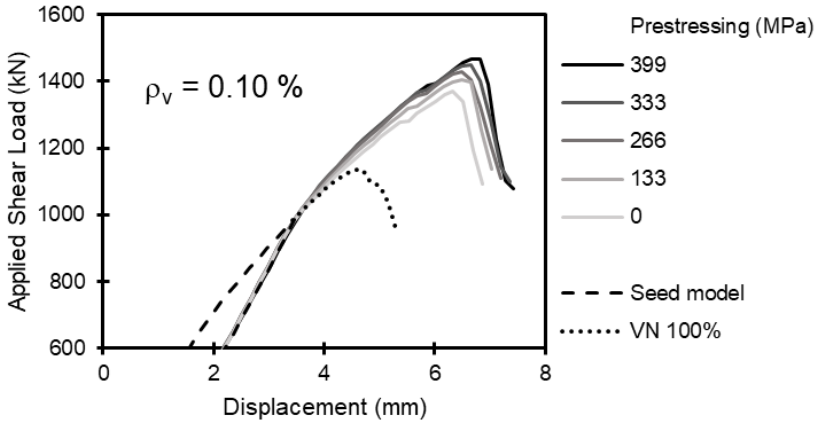



**Figure 3.8.** Influence of prestressing level (VN seed model)

**Table 3.3.** Peak shear capacity and influence of prestressing level

| Prestressing (MPa) | 0 | 66.5 | 133 | 199 | 266 | 333 | 399 | 465 | 532 |
|---|---|---|---|---|---|---|---|---|---|
| Equivalent prestrain ($\times 10^{-3}$) | 0 | 0.5 | 1.0 | 1.5 | 2.0 | 2.5 | 3.0 | 3.5 | 4.0 |
| Shear capacity (kN) | 1370 | 1386 | 1406 | 1420 | 1429 | 1450 | 1466 | 1475 | 1475 |
| Shear strength increase (%) | 21 | 22 | 24 | 25 | 26 | 28 | 29 | 30 | 30 |

### 3.4.2 Crack Closing Potential

Figure 3.9 shows the computed crack closing response of a single finite element that is estimated to occur as a result of clamping action developed by way of the active prestressing. The selected element was located at one of the shear cracks of the seed model before retrofit, as shown in Figure 3.10. The effectiveness of the Fe-SMA retrofits in closing shear cracks is clearly evident in even the lowest volume of external reinforcement. As the reinforcement ratio increases, shear crack widths are reduced by up to 88 %.

The influence of prestressing level on the cracking reduction is clearly apparent in Figure 3.10, with estimated shear crack widths being significantly smaller for retrofits employing higher prestressing levels (e.g., 399 MPa). Moreover, a major benefit of introducing transverse prestressing in the RC beams is the potential that cracking may be better-controlled and mitigated such they are closed, and remain small, under routine service load levels. Overall, the findings of these numerical results indicate that the presence of externally bonded Fe-SMA retrofits is able to provide significant improvements in the shear resisting performance of large-scale RC beams. However, further experimental research is required to establish the viability of the proposed method and to explore different bonding techniques to incorporate Fe-SMA into the surface of the concrete.

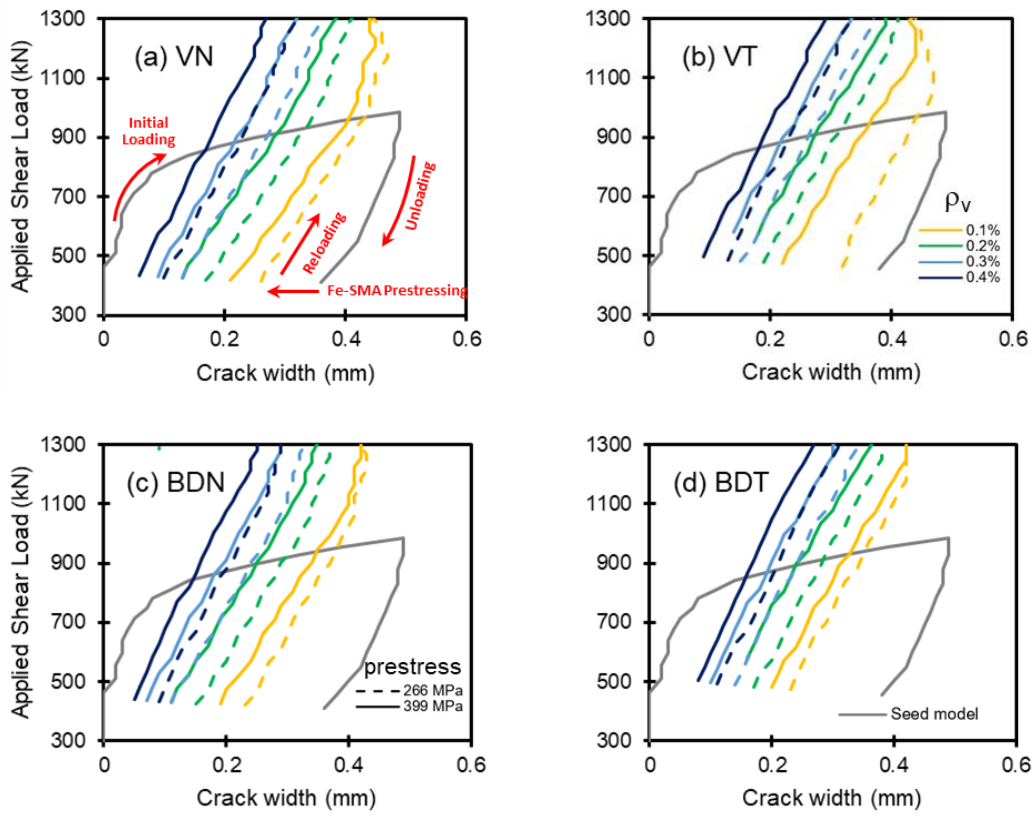



**Figure 3.9.** Crack width in a single element




**Figure 3.10.** Crack widths in test span before prestressed Fe-SMA addition

## 3.5 Summary

A numerical study was conducted to evaluate the influence of several parameters on the shear resisting performance of RC beams. The results of this investigation showed that the presence of prestressed Fe-SMA on the surface of the beams can provide several improvements, which are summarized as follows:

- Fe-SMA retrofits were estimated to provide stiffness and strength improvements in damaged RC components as a result of the transverse prestressing induced by way of the active retrofit strategy.
- In the same manner as expected with similar retrofit methods involving passive techniques, the shear capacity of damaged shear-critical beams was estimated to increase as more transverse reinforcement was provided. Combinations of large shear reinforcement ratios with high levels of transverse prestressing provided the largest shear strength gains.
- The additional of prestressed Fe-SMA retrofits were estimated to reduce (i.e., close) shear crack widths and mitigate the development of subsequent shear crack width growth.

# Chapter 4
# Experimental program

## 4.1 General

An experimental program was developed to investigate the effectiveness of thermally activated Fe-SMA shear retrofit on RC. The experimental program for this study consisted of three phases:

1) Characterization of reinforcement materials (conventional steel rebar and Fe-SMA).
2) Recovery stress testing of the Fe-SMA reinforcement.
3) Push-off testing of Fe-SMA retrofitted RC specimens.

This chapter presents the testing of eight Fe-SMA strips to determine the ideal combination of prestrain and temperature that provides the greatest gains in terms of recovery stress, and the testing of four RC push-off specimens under uniaxial monotonic load to evaluate the potential of using external prestressed Fe-SMA retrofits. The following sections describe the concrete mixture used, the methods used to characterize metallic materials and provide the results of the characterization tests. The recovery stress and push-off tests are described in detail, including the purpose of the tests, the test setup, equipment used, and data collection methods. The push-off test section includes information on the test specimens, the instrumentation used to measure load and displacement, the experimental procedure, and the test matrix.

## 4.2 Material Characterization

In this section, a thorough characterization of the key materials used in the experimental program will be provided, aiming to understand their individual contributions to the overall behaviour of the push-off specimens. The characterization of materials involved identifying the properties of the concrete mix, as well as conducting tensile tests on coupon specimens to assess the mechanical behaviour of the steel reinforcement and Fe-SMAs. This comprehensive analysis lays the foundation for a well-informed interpretation of the experimental results and the effectiveness of the shear strengthening method.

The characterization of materials involved identifying the properties of each component used in the concrete mix. Additionally, the steel reinforcement and Fe-SMA were characterized through tensile tests on coupon specimens.

### 4.2.1 Concrete Mixture

The concrete mixture was designed to achieve the desired properties, ensuring that push-off specimens would exhibit the required strength and durability. The mix consisted of conventional concrete constituent materials, utilizing a maximum nominal size of coarse aggregate of 20 mm. The mix design ratios included 1 unit of Portland-limestone (GUL) cement to 1.9 units of fine aggregate (sand) and 2.5 units of coarse aggregate (i.e., a ratio of 2.5-1.9-1) and was cast using a water-cement ratio of 0.51. The choice of Portland-limestone cement provided not only adequate strength but also contributed to reducing the carbon footprint. To optimize the workability of the mix, two types of admixtures were incorporated. A water reducer was added at a proportion of 0.39 ml/kg of cement, while a superplasticizer was introduced at a proportion of 0.42 ml/kg of cement. These admixtures effectively improved the flowability and cohesiveness of the concrete, facilitating its placement and consolidation during the casting process.

After preparation of the mix, it was cast within a steel form, and immediate action was taken to ensure proper compaction. Vibrating the concrete mix helped eliminate excessive entrapped air and enhanced the concrete's density and uniformity. This step was crucial in avoiding potential voids or weak zones that could compromise the structural integrity of the specimens. Following casting and compaction, the concrete specimens were subjected to compressive strength tests following the ASTM C31 and C39 standards (American Society for Testing and Materials, 2019, 2021). The testing program involved three cylinders for each age, tested at: 7 days, 14 days, and the day of the push-off testing. Results for the compressive strength are summarized in Table 4.1. This comprehensive approach allowed the evaluation of the concrete's strength development over time.

**Table 4.1.** Summary of compressive test on concrete cylinders.

| Specimen | Average compressive strength (MPa) | | |
|---|---|---|---|
| | Age | | |
| | 7 days | 14 days | Testing day |
| Specimen A | 30.3 | 35.5 | 40.8 (81)[1] |
| Specimen B | 25.4 | 31.6 | 33.5 (80)[1] |
| Specimen C | 23.5 | 27.8 | 31.1 (80)[1] |
| Specimen D | 25.6 | 30.8 | 35.4 (84)[1] |

[1]age of test specimens at time of RC push-off specimen testing

### 4.2.2 Steel Reinforcement

The push-off specimens used in the experiments were reinforced both longitudinally and transversely to ensure optimal performance under the applied loads. For the longitudinal reinforcement, grade 400W 20M and 10M bars were utilized. The 10M bars were employed as double-legged closed stirrups, providing lateral confinement to the concrete. Additionally, 3/16” cold-rolled solid rounds were strategically placed to cross the shear plane, providing an intentional minimal amount of interface shear reinforcement. This comprehensive arrangement aimed to enhance the specimen's flexural and shear capacities, ensuring its ability to resist applied loads and prevent premature failures.

To validate the properties of the reinforcement steel, a rigorous characterization was performed through tensile tests following the ASTM E8 standard (American Society for Testing and Materials, 2022). The tests allowed for evaluation of critical mechanical properties, such as yield strength and ultimate tensile strength. Three samples were tested for each type of reinforcement and the results of the tensile tests, including the mechanical properties of the reinforcement steel, are summarized in Table 4.2, providing essential data to ensure the suitability of the reinforcement for its intended use in the push-off specimens.

The test setup for the reinforcement steel characterization, depicted in





(a) Test setup (b) Tensile failure

**Figure 4.1**, ensured accurate and reliable measurements during the tensile tests, employing an extensometer to measure the strain in the samples. These characterization tests were of paramount importance to verify that the reinforcement steel met the required mechanical properties, ensuring it could provide the necessary strength and ductility to withstand the applied loads effectively.

**Table 4.2.** Material Properties of Reinforcement Steel

| Bar | Diameter (mm) | Area ($mm^2$) | Modulus of Elasticity | | Yielding Stress | | Ultimate Strength | |
|---|---|---|---|---|---|---|---|---|
| | | | (GPa) | COV | (MPa) | COV | (MPa) | COV |
| 20M | 19.5 | 300 | 194 | 0.03 | 529 | 0.01 | 620 | 0.01 |
| 10M | 11.3 | 100 | 190 | 0.02 | 520 | 0.01 | 682 | 0.01 |
| 3/16" | 4.76 | 17.8 | 205 | 0.03 | 1060 | 0.02 | 1,232 | 0.01 |





(c) Test setup (d) Tensile failure

**Figure 4.1.** Tensile test on reinforcement bars

### 4.2.3 Fe-SMA strips

The Fe-SMA (Fe-17Mn-5Si-5Cr-4Ni-0.1C alloy) in this study was developed by Hong et al. (2020). The Fe-SMA was obtained in plate-form with a length of 1870 mm, a width of 204 mm and a thickness of 3 mm. The plate was cut in to 2.5 mm × 1600 mm strips using a waterjet. The resulting strips were then used for the recovery stress and push-off tests.

To characterize the Fe-SMA, dogbone-shaped specimens were cut from the Fe-SMA plate and tested for tensile capacity following ASTM standard E8 (American Society for Testing and Materials, 2022). The dimensions of the specimens used were based on the standard requirements, as shown in Figure 4.2. Two tensile tests were conducted using a universal testing machine, with a crosshead speed of 2 mm/min (Figure 4.3). The load and displacement data were recorded, and the tensile capacity of the Fe-SMA was determined. The test results are reported in Table 4.3, which includes the mean values for elasticity modulus, yield strength and ultimate strength of the Fe-SMA with a COV of 0.03 for the three parameters.

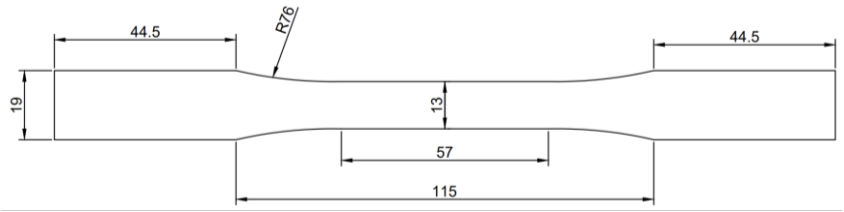



**Figure 4.2.** Fe-SMA tensile test specimen (dimensions in mm)

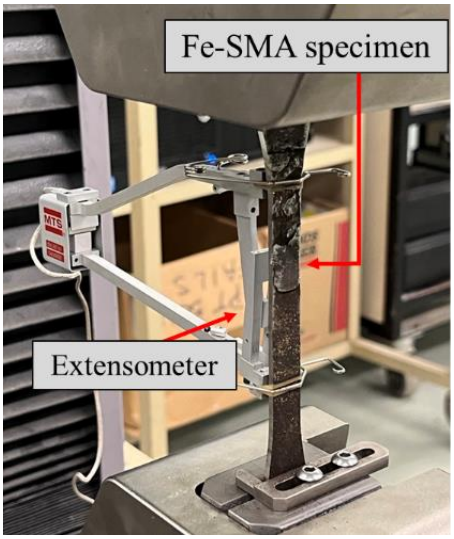


**Figure 4.3.** Fe-SMA tensile test setup

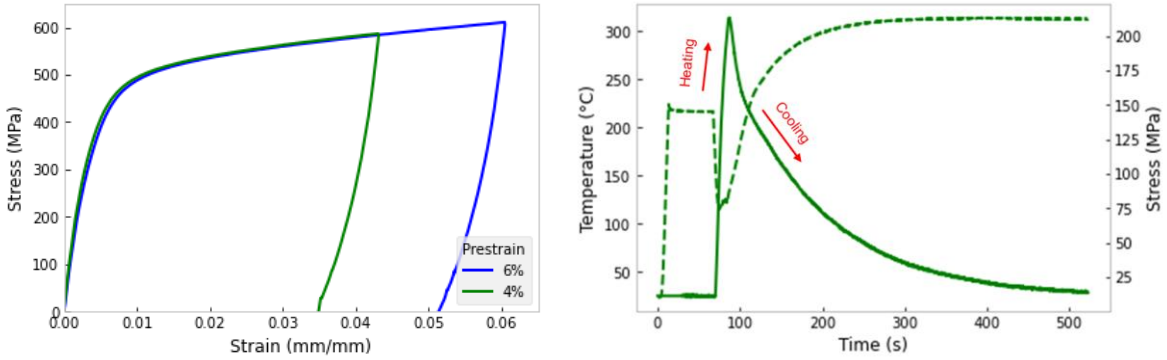
**Table 4.3.** Material Properties of Iron-based Shape Memory Alloy

| Modulus of Elasticity (GPa) | Yielding Stress (MPa) | Ultimate Strength (MPa) |
|---|---|---|
| 103 | 455 | 654 |

## 4.3 Recovery Stress Tests

The second phase of the experimental program focused on conducting the recovery stress test. The main objective of this phase was to observe the behaviour of the deformed Fe-SMA strip when subjected to heating and to identify the most effective combination of prestressing and temperature that would lead to the highest recovery stress. In this test, 2.5 mm × 3 mm strips were cut, each Fe-SMA strip was initially deformed in tension using an MTS C45 testing frame until reaching the desired strain level (Figure 4.4a). After achieving the desired strain, the strip was unloaded, leaving a certain amount of plastic deformation in the sample.

Subsequently, the sample was placed back into the testing frame, and a 150 MPa load was applied to prevent any potential buckling during the test. The next step involved applying an electric current through a power supply unit to heat the Fe-SMA strip. As the strip underwent phase transformation to regain its original shape, it generated internal stress, known as recovery stress. A schematic view of the heating and cooling process is illustrated in Figure 4.4b. The stress recorded at the end of the test represents the recovery stress developed during the heating-cooling process.




(a) Pre deformation phase (b) Temperature and stress over time

**Figure 4.4.** Recovery stress test phases

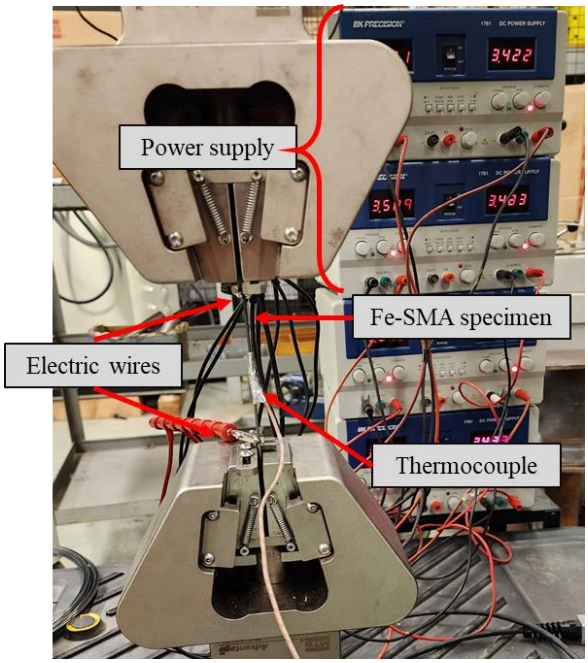



**Figure 4.5.** Recovery stress test setup

The experimental setup, as shown in Figure 4.5, consisted of a MTS C45 testing frame equipped with a load cell, an electric power supply unit, and a thermocouple to measure temperature. The Fe-SMA strips were cut to a length of 180 mm using a bandsaw. A total of 8 strips were subjected to the test, with each strip tested at varying temperature values. To achieve different temperature levels, the amperage values were adjusted between 28A and 60A, resulting in temperatures ranging from 200˚C to 320˚C for the Fe-SMA strips. These temperatures corresponded to strain levels of 4% and 6%. Throughout the test, the temperature variation along the strip was monitored using a thermocouple connected at the midspan of the strip.

## 4.4 Push-Off Tests

The objective of this phase is to investigate the effectiveness of self-prestressed Fe-SMA strips as a shear retrofit on damaged RC specimens via push-off testing. This section includes the geometry of the specimens, details of the reinforcement used, a test matrix, and a description of the experimental procedure. The experimental procedure involved a precracking of the specimens along the shear crack plane, a Fe-SMA retrofit with strips prestrained to a desired strain level, activation of the shape memory effect, and loading of the retrofitted specimen with an actuator.

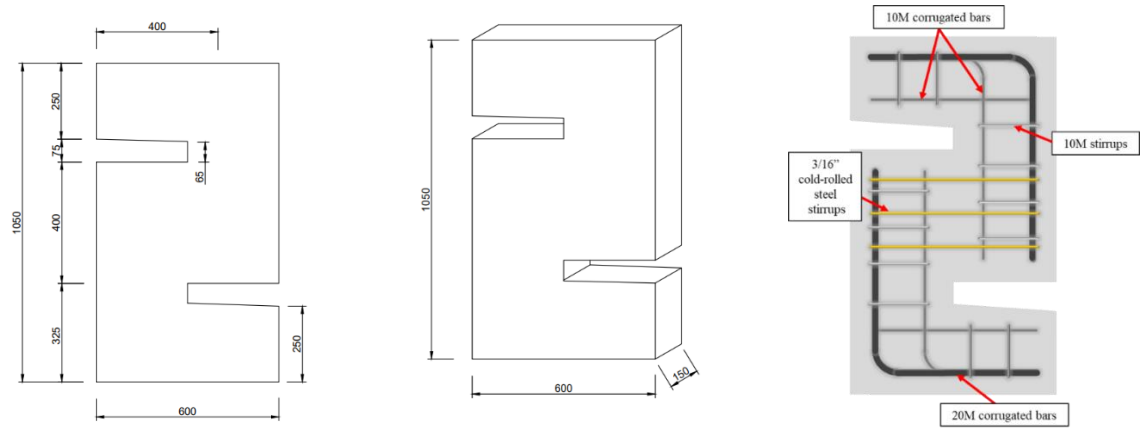


**Figure 4.6.** Push-off specimen

Push-off specimens (Figure 4.6) have traditionally been used to evaluate the shear strength and evaluate shear transfer mechanisms. These small specimens provide an accurate understanding of the load transfer mechanism and allow a larger experimental campaign compared to full-scale specimens. Additionally, push-off specimens have been employed to identify the direct shear transfer mechanism and to better understand the behaviour on the interface through experimental tests. Although the push-off test is nonstandard, it is a widely recognized experimental test used to accurately study shear transfer mechanisms.

### 4.4.1 Test Specimen

The push-off specimens utilized in this study have a distinctive Z-shape configuration, with dimensions measuring 600 mm in width, 1000 mm in height, and 150-mm thick. The geometric details and reinforcement layout of these specimens are illustrated in Figure 4.7. Preparation of the steel reinforcement cages, and formwork are shown in Figure 4.8.




(a) push-off geometry (dimensions in mm) (b) reinforcement details

**Figure 4.7.** Push-off specimen details



**Figure 4.8.** Rebar cages preparation

### 4.4.2 Test Matrix

The experiments were performed to examine the behaviour of RC push-off specimens externally self-prestressed with Fe-SMA strips. Four push-off specimens were cast. One of the specimens was used as a baseline and was constructed without any form of retrofit. Two specimens were externally retrofitted with self-prestressed Fe-SMA strips at reinforcement ratios of 0.2 % and 0.4 % with respect to the shear plane and the remaining specimen was retrofitted with non-activated Fe-SMA. Table 4.4 summarizes the parameters studied in these experiments.

**Table 4.4.** Test matrix

| Specimen | Fe-SMA Reinforcement Ratio | Number of Strips | Fe-SMA Spacing (mm) | Activation | Active Confinement Pressure (MPa) | |
|---|---|---|---|---|---|---|
| | | | | | $f_{l,x}$ | $f_{l,y}$ |
| A (Control) | N/A | N/A | N/A | N/A | N/A | N/A |
| B | 0.2 % | 8 | 40 | Activated at 200˚C | 0.27 | 0.07 |
| C | 0.4 % | 16 | 22.2 | Activated at 200˚C | 0.54 | 0.13 |
| D | 0.2 % | 8 | 40 | Non-activated | N/A | N/A |

The active confinement pressure provided by the Fe-SMA external reinforcement in both directions of the rectangular section was calculated using equations (1) to (3) as suggested by Mander et al. (1988).

$$f_{l,x} = \frac{k_e A_{SMA}}{s_{SMA} d} \sigma_r \quad \textbf{(1)}$$

$$f_{l,y} = \frac{k_e A_{SMA}}{s_{SMA} b} \sigma_r \quad \textbf{(2)}$$

$$k_e = \left(1 - \frac{s'}{2b}\right)\left(1 - \frac{s'}{2d}\right) \quad \textbf{(3)}$$

Where $A_{SMA}$ is the cross-sectional of Fe-SMA strips, $s_{SMA}$ is the centre-to-centre spacing of Fe-SMA strips, $s'$ is the clear spacing between the strips, $b$ and $d$ are the width and thickness of the push-off specimens respectively, $k_e$ is a correction factor to account for unconfined regions of concrete and $\sigma_r$ is the recovery stress of the Fe-SMA based on the results presented in section 5.2, for a 4 % prestrain and heated to 205°C.

### 4.4.3 Test Setup and Instrumentation

The test setup for the push-off experiments in this study involved an MTS 311 frame, which allowed for vertical loading of the specimens. Load and displacement measurements were recorded using a load cell integrated within the testing frame, providing real-time data acquisition during testing. Additionally, three linear variable differential transformers (LVDT) were positioned to measure average cracks and slip displacements on one face of the specimens (see Figure 4.9). The combined use of the MTS 311 frame, load cell, and LVDTs ensured accurate and comprehensive testing, enabling a thorough assessment of the Fe-SMA shear retrofit effectiveness and the overall performance of the push-off specimens.

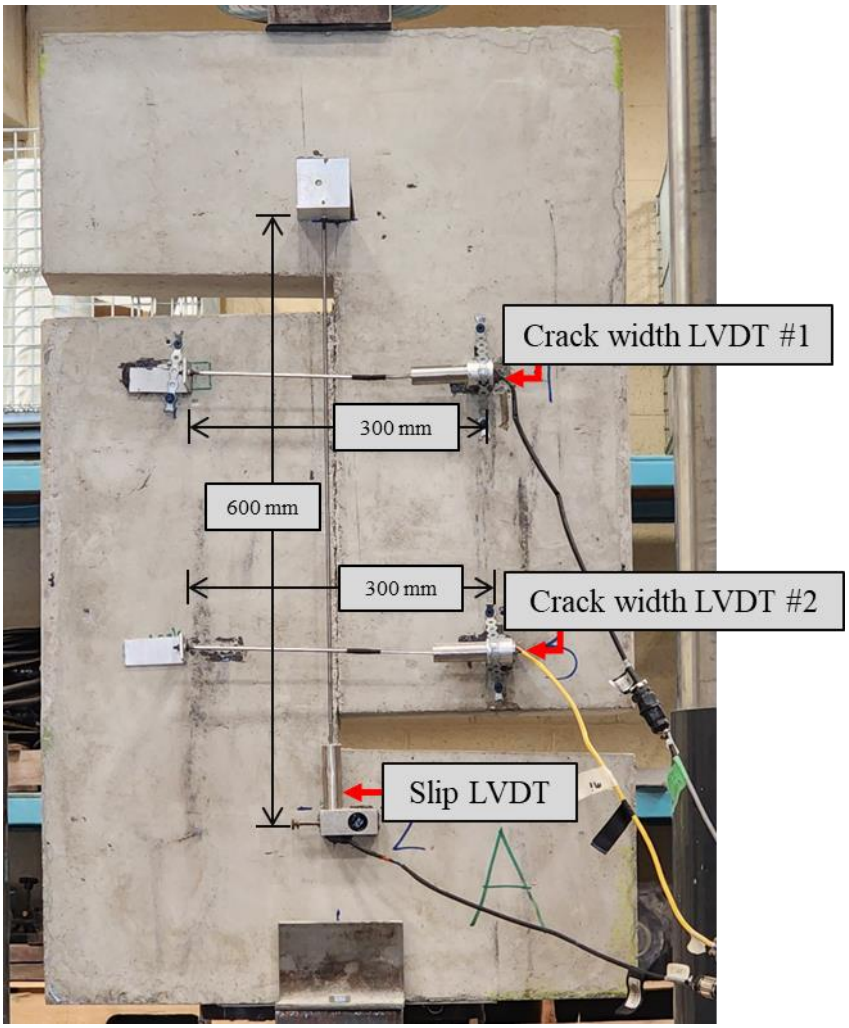



**Figure 4.9.** Instrumentation (LVDT) layout

### 4.4.4 Test Procedure

The push-off testing procedure consisted of three main phases. In the initial phase, precracking was induced along the shear plane of the specimen using a 500-kN testing frame (Figure 4.10). This precracking ensured the presence of a well-defined shear crack in the specimen before the retrofitting process. To transfer the load, steel angles were placed at the top and bottom of the specimen, ensuring

uniform distribution along the length equal to the shear plane. Extruded polystyrene foam blocks were strategically utilized to maintain the specimen balanced on the angles during the precracking process.

In the second phase of the experiment, the retrofitted specimen underwent meticulous preparation with predeformed Fe-SMA strips, each measuring 2.5 mm in width and 1.5 m in length. These Fe-SMA strips were subjected to a 4 % strain and posteriorly unloaded using a testing frame. Following this predeformation, the strips were wrapped around the designated section of the specimen. To ensure optimal adhesion to the concrete surface, the corners of the push-off specimen were rounded through grinding. The Fe-SMA strips were securely held in place utilizing U-bolt clamps, and to impart initial tension to the strips, a turnbuckle connection was employed (Figure 4.11a). Subsequently, the activation process was initiated using a power supply unit, applying an amperage of 50 A for three minutes until the Fe-SMA strips reached an approximate temperature of 200°C. This activation led to the phase transformation of the Fe-SMA material, causing it to exert internal stresses and generate recovery forces, contributing to the overall strengthening of the retrofitted specimen.



(b) Precracking test setup (b) Bearing angles (c) Cracked specimen

**Figure 4.10.** Precracking phase



(a) Turnbuckle connection installation



(b) Fe-SMA retrofitted specimen



(c) Fe-SMA on specimen C before activation



(d) Specimens B, D and C



(e) Activated Fe-SMA on specimen B



(f) Fe-SMA activation

**Figure 4.11.** Fe-SMA on precracked specimens

The final phase involved the vertical loading of the precracked and retrofitted push-off specimens (Figure 4.12). Vertical forces were applied to the bottom of the specimen while the opposing surface (i.e., the top) of the specimen was vertically-restrained, inducing shear loading conditions. Over the course of push-off testing, load and displacement measurements were continuously recorded using instrumentation equipped with the MTS 311 frame, and crack widths and slip were measured with LVDTs ensuring accurate and real-time data acquisition. To ensure precise vertical loading, specimens were prepared by grinding at the designated bearing plate locations to achieve a thoroughly perpendicular orientation during the loading process (Figure 4.13).

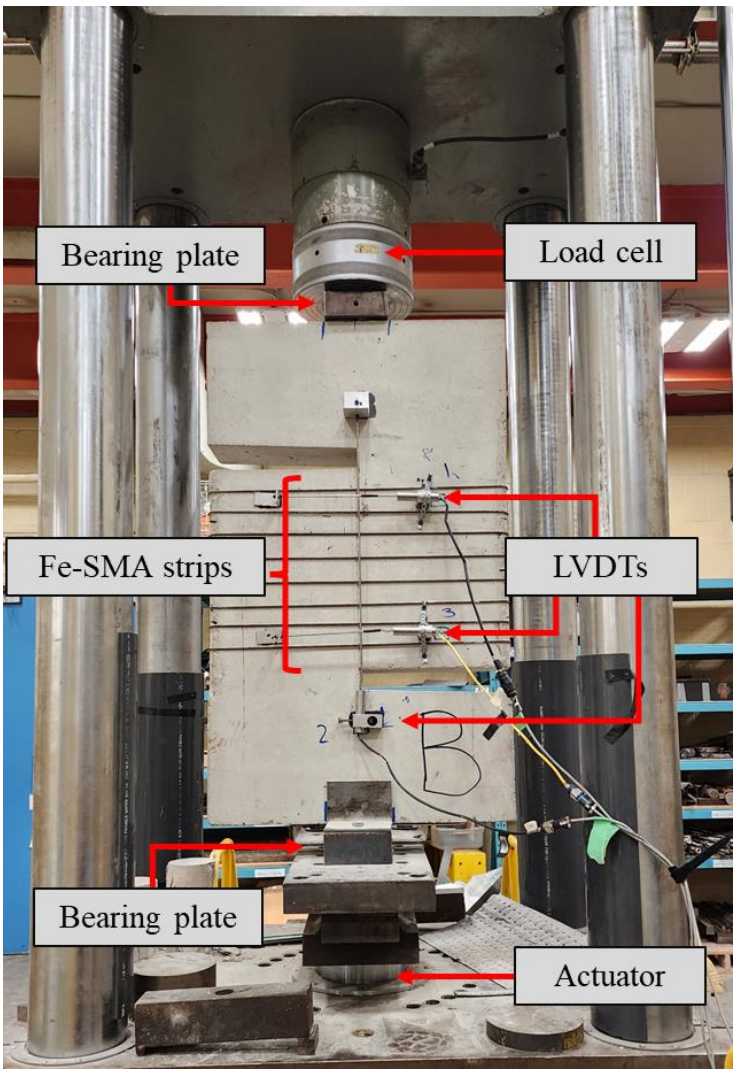



**Figure 4.12.** Push-off test setup



**Figure 4.13.** Bearing surface grinding

# Chapter 5
# Experimental Results and Discussion

## 5.1 General

This chapter provides an overview of the experimental procedures conducted in the study. As described in Chapter 3, these procedures encompassed recovery stress tests and push-off tests. The chapter is dedicated to presenting and discussing the outcomes of these tests, which were designed to evaluate the feasibility and effectiveness of utilizing Fe-SMAs as an active retrofitting technique for shear-critical RC components. The results are presented systematically, focusing on various aspects, including recovery stress, precracking, shear stress, crack slip displacements, crack widths and the overall performance and practicality of Fe-SMA in enhancing the shear capacity of these structural elements.

## 5.2 Recovery Stress Results

A total of eight Fe-SMA strips were tested (Figure 5.1). These specimens were conditioned with two different prestrain levels, 4 % and 6 %, and were tested at varying temperatures. The analysis consistently showed that temperature has a significant impact on the generation of recovery stress. The Fe-SMA specimens demonstrated an increasing trend in recovery stress as the temperature increased. The maximum recovery stress recorded for specimens with 4 % prestrain was 294 MPa, whereas for specimens with 6 % prestrain, 287 MPa. This data highlights the temperature sensitivity of recovery stress in Fe-SMA materials and the slightly better performance at the 4% prestrain level. The final recovery stresses obtained during the test are presented in Table 5.1.

**Table 5.1.** Recovery stress at the end of the test

| **4 % Prestrain** | | **6 % Prestrain** | |
|---|---|---|---|
| **Max. Temperature (˚C)** | **Recovery Stress (MPa)** | **Max. Temperature (˚C)** | **Recovery Stress (MPa)** |
| 205 | 259 | 196 | 226 |
| 225 | 268 | 221 | 252 |
| 268 | 275 | 253 | 269 |
| 320 | 294 | 321 | 287 |

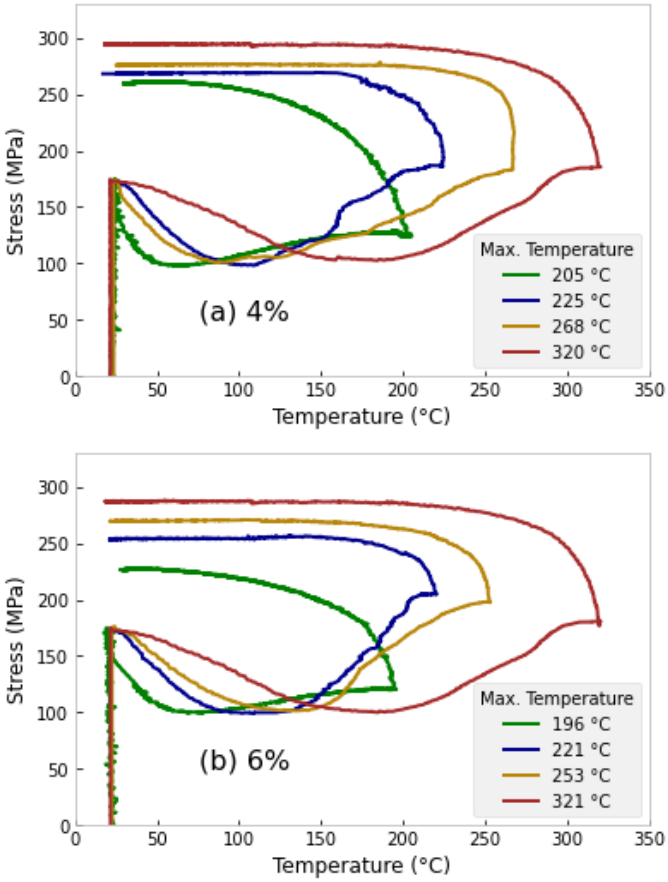



**Figure 5.1.** Recovery stress test results

## 5.3 Push-Off Results

In this section, the results of the push-off tests are presented and analyzed. A total of four RC push-off specimens were tested (as described in Table 4.4), each configured as illustrated in Figure 5.2. These tests aimed to investigate the behaviour of the retrofitted specimens under interface shear loading conditions. The analysis begins with an examination of the precracking development in the specimens. The precracking loads for each specimen are presented in Table 5.2.

**Table 5.2.** Precracking stage peak loads.

| **Specimen** | **A** | **B** | **C** | **D** |
|---|---|---|---|---|
| **Cracking load (kN)** | 159 | 141 | 141 | 151 |




(a) Specimen A (Control)




(b) Specimen B (0.2 % Activated Fe-SMA)




(c) Specimen C (0.4 % Activated Fe-SMA)




(d) Specimen D (0.2 % Non-activated Fe-SMA)

**Figure 5.2.** Push-off specimens

The results of the push-off tests are presented in terms of axial load and shear stress, which is calculated using Equation 4,

$$\tau = \frac{P}{h_{sp} b_{sp}} \quad \textbf{(4)}$$

where $h_{sp}$ is the shear plane depth (400 mm) and $b_{sp}$ is the shear plane width (150 mm). Additionally, data on crack widths, measured through readings from horizontal LVDTs, and crack slip displacements, determined using vertical LVDTs, are presented.

### 5.3.1 Peak Load

The peak loads achieved during the push-off tests serve as a key indicator of the effectiveness of the Fe-SMA retrofitting technique. Figure 5.3 illustrates the results in terms of axial load. Moreover, a summary of the peak loads is presented in Table 5.3. Most apparent and most notable, it can be observed that the specimens retrofitted with Fe-SMA consistently exhibited higher peak loads compared to non-retrofitted and passive retrofitted counterparts, demonstrating the capacity of the Fe-SMA retrofit to enhance the shear resistance of the RC specimens. The condition of each specimen after push-off testing is presented in Figure 5.4

**Table 5.3.** Push-off peak loads

| **Specimen** | **A** | **B** | **C** | **D** |
|---|---|---|---|---|
| **Peak load (kN)** | 155 | 207 | 244 | 173 |

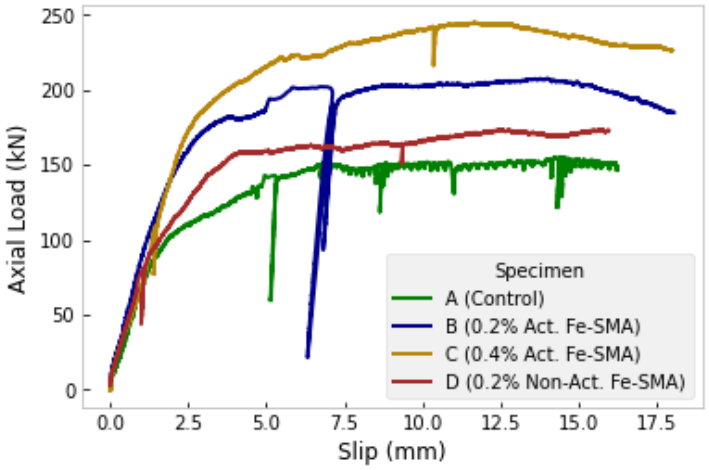
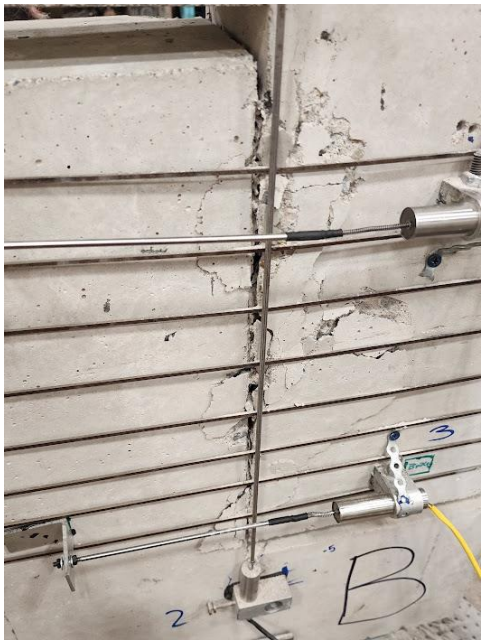



**Figure 5.3.** Axial load vs measured slip results



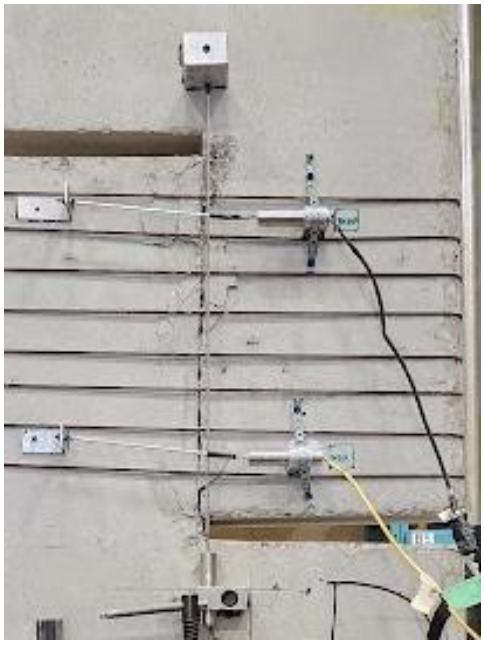
(a) Specimen A (Control)




(b) Specimen B (0.2 % Activated Fe-SMA)



(c) Specimen C (0.4 % Activated Fe-SMA)

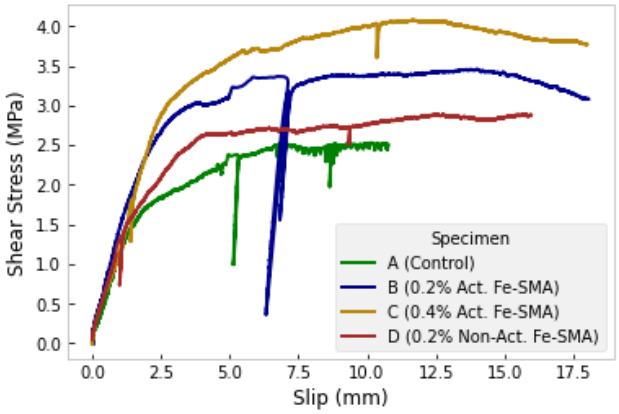


(d) Specimen D (0.2 % Non-activated Fe-SMA)

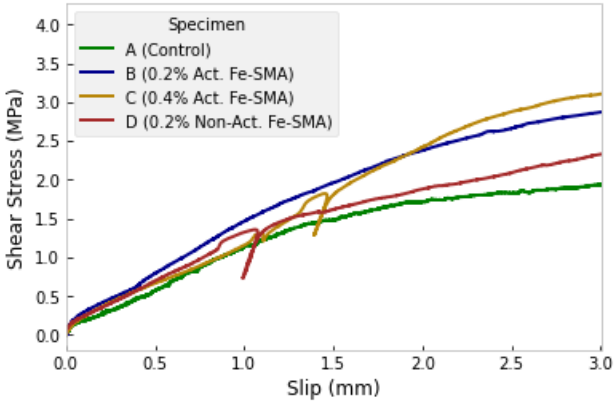
**Figure 5.4.** Shear plane after failure

### 5.3.2 Shear Stress – Slip

The relationship between shear stress and shear slip, a critical aspect of the push-off tests, provides valuable insights into the performance of the retrofitted concrete specimens. Results for this relationship are presented in Figure 5.5. Notably, specimens A and D exhibit a reduction in stiffness within the range of 1.0 to 1.5 MPa, followed by reaching a maximum load and transitioning into a plateau phase where slip continues to increase. This phenomenon can be attributed to the high yielding stress of the internal reinforcement crossing the shear plane, which continues to yield even after the specimen has failed. Conversely, for actively retrofitted specimens B and C, the initial stiffness slope remains well-maintained, extending up to 2.5 MPa. Additionally, it's noteworthy that an increase in the reinforcement ratio correlates with higher shear stress at failure, indicating the significance of reinforcement in shear performance enhancement. This trend was consistent with the results obtained from section 3.4.1




(a) Full response




(b) Measured slip range between 0 and 3 mm

**Figure 5.5.** Shear stress vs slip results

### 5.3.3 Shear Stress – Crack Width

Results in terms of shear stress and crack width are presented in Figure 5.6. It is important to note that due to technical issues, only one horizontal LVDT was employed for recording shear plane crack width readings. The crack widths were initially at zero, as they were induced during the precracking phase of the test. Throughout the test, an interesting trend emerges: Specimen D, which was passively retrofitted, shows only minor improvements in controlling crack width development as the level of applied shear stress increases. In contrast, the actively retrofitted specimens exhibited more controlled crack width development, particularly in the shear stress range of up to 2.5 MPa. These observations underscore the effectiveness of active retrofitting in mitigating crack width development.

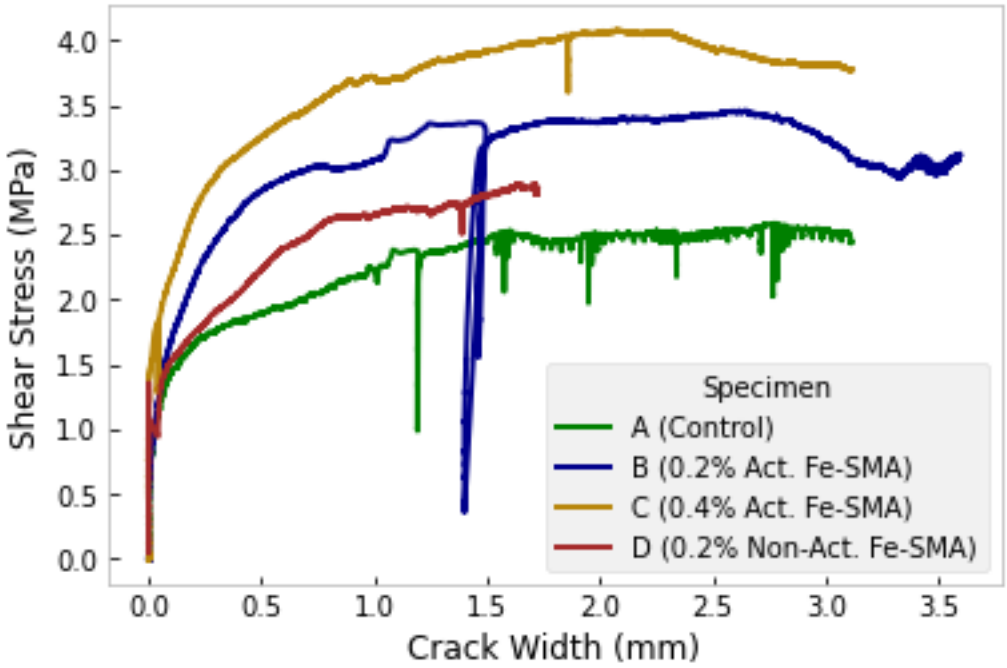



**Figure 5.6.** Shear stress vs crack width results

### 5.3.4 Self-Prestressing and Shear Behaviour Enhancement

The findings from the experimental results yield valuable insights into the behaviour of the retrofitted specimens and the efficacy of the Fe-SMA retrofitting technique. One notable aspect is the self-prestressing effect, which plays a role in enhancing the overall performance of the retrofitted specimens. This effect is particularly significant in actively retrofitted specimens, where the confinement provided by the Fe-SMA strips actively contributes to resisting shear forces. As a result, the actively retrofitted specimens (B and C) exhibited improved shear capacity and more controlled crack widths compared to the passively retrofitted test specimen (D).

The enhancements in shear capacity are especially noteworthy, with the actively retrofitted specimens showing higher peak loads and maintaining their stiffness over a wider range of shear stress. This demonstrates the ability of the Fe-SMA retrofitting to effectively strengthen the shear-deficient RC members. Moreover, the crack control observed in actively retrofitted specimens is a critical advantage. The Fe-SMA retrofitting technique not only increases the shear capacity but also helps prevent excessive crack development. This is particularly beneficial for maintaining the structural integrity, durability, and long-term performance of RC elements.

In summary, the results highlight the promising potential of Fe-SMA retrofitting in enhancing shear capacity, controlling crack widths, and contributing to the overall resilience of RC structures subjected to shear forces.

# Chapter 6
# Conclusions and Recommendations

## 6.1 General Remarks

This study investigated the effectiveness of Fe-SMAs as an innovative retrofitting technique for shear-critical RC elements. The comprehensive experimental program, consisting of recovery stress tests and push-off tests, along with FEA simulations, have provided significant insights into the application of using Fe-SMA retrofits for enhancing the capacity of shear-critical elements, controlling crack development, and, as a result, its potential contributions to enhancing the resilience and durability of RC structures. Several key findings and general remarks emerged from this research:

- **Self-Prestressing Effect:** The Fe-SMA retrofitting technique demonstrated a remarkable self-prestressing effect when activated. The Fe-SMA strips, upon phase transformation, generated internal stresses and recovery forces, contributing substantially to the enhanced shear capacity of the retrofitted specimens. This self-prestressing phenomenon holds promise for improving the load-bearing capacity of shear-deficient RC structures.
- **Shear Capacity Enhancement:** The actively retrofitted specimens exhibited notable enhancements in shear capacity compared to passively retrofitted, and non-retrofitted ones. Displaying higher peak loads and maintaining initial stiffness over a broader range of shear stress levels. This suggests that Fe-SMA retrofitting can effectively strengthen shear-critical RC elements, making them more resilient to shear forces.
- **Crack Control:** In addition to increased shear capacity, actively retrofitted specimens demonstrated effective crack control. The Fe-SMA retrofitting technique was shown to effectively control the development of cracks under increasing shear stress levels. This is a crucial advantage for preserving the structural integrity and long-term performance of RC elements subjected to shear forces.

## 6.2 Recommendations for Future Work

While this study has provided notable remarks into the feasibility and potential benefits of Fe-SMA retrofitting, there are several avenues for future research to explore and enhance the applicability of this innovative technique:

- **Bonding Alternatives:** Exploring alternative bonding methods and materials for Fe-SMA retrofitting warrants further investigation. Different adhesives and anchorage systems may offer improved performance and durability, addressing potential concerns related to environmental exposure and long-term effectiveness.
- **Field-Representative Tests:** To validate the findings of this research in real-world scenarios, conducting field-representative tests on larger-scale structures is recommended. Field tests can provide a more accurate assessment of the Fe-SMA retrofitting technique's performance and practicality under diverse environmental and loading conditions.

In conclusion, this study has advanced the understanding of Fe-SMA retrofitting as an active shear-strengthening technique for RC structures. The self-prestressing effect, shear capacity enhancement, and crack control demonstrated in this research underscore the potential of Fe-SMA retrofitting to enhance the resilience and durability of shear-critical RC elements. By addressing the recommended areas of future work, engineers and researchers can further refine and expand the application of this innovative retrofitting approach in the field of structural engineering.

# References


Adhikary, B. B., Mutsuyoshi, H., & Sano, M. (2000). Shear strengthening of reinforced concrete beams using steel plates bonded on beam web: experiments and analysis. In *Construction and Building Materials* (Vol. 14).

Al-Mahmoud, F., Castel, A., Quang Minh, T., & François, R. (2015). Reinforced Concrete Beams Strengthened with NSM CFRP Rods in Shear. *Advances in Structural Engineering*, *18*(10).

Altin, S., Anil, Ö., & Kara, M. E. (2005). Improving shear capacity of existing RC beams using external bonding of steel plates. *Engineering Structures*, *27*(5), 781–791. https://doi.org/10.1016/j.engstruct.2004.12.012

American Association of State Highway and Transportation Officials. (2019). *AASHTO LFRD Bridge Design Specifications*.

American Concrete Institute. (2019). *Building Code Requirements for Structural Concrete (ACI 318-19)*.

American Society for Testing and Materials. (2019). *ASTM C31/C31M Standard Test Method for Splitting Tensile Strength of Cylindrical Concrete Specimens 1*. https://doi.org/10.1520/C0496_C0496M-17

American Society for Testing and Materials. (2021). *ASTM C39/C39M Standard Test Method for Compressive Strength of Cylindrical Concrete Specimens*. https://doi.org/10.1520/C0039_C0039M-21

American Society for Testing and Materials. (2022). *ASTM E8/E8M Standard Test Methods for Tension Testing of Metallic Materials*. https://www.astm.org/e0008_e0008m-22.html

Buehler, W. J., Gilfrich, J. V., & Wiley, R. C. (1962). Effect of Low-Temperature Phase Changes on the Mechanical Properties of Alloys near Composition TiNi. *Journal of Applied Physics*, *34*(5), 1475. https://doi.org/10.1063/1.1729603

Canadian Standards Association. (2019a). *CSA A23.3:19, Design of concrete structures*. CSA Group.

Canadian Standards Association. (2019b). *CSA S6:19, Canadian Highway Bridge Design Code*. CSA Group.

Chalioris, C. E., & Pourzitidis, C. N. (2012). Rehabilitation of Shear-Damaged Reinforced Concrete Beams Using Self-Compacting Concrete Jacketing. *ISRN Civil Engineering*, *2012*, 1–12. https://doi.org/10.5402/2012/816107

Cladera, A., Montoya-Coronado, L. A., Ruiz-Pinilla, J. G., & Ribas, C. (2020). Shear strengthening of slender reinforced concrete T-shaped beams using iron-based shape memory alloy strips. *Engineering Structures*, *221*. https://doi.org/10.1016/j.engstruct.2020.111018

Cladera, A., Weber, B., Leinenbach, C., Czaderski, C., Shahverdi, M., & Motavalli, M. (2014). Iron-based shape memory alloys for civil engineering structures: An overview. *Construction and Building Materials*, *281*, 281–293. https://doi.org/10.1016/j.conbuildmat.2014.04.032

Czaderski, C., Shahverdi, M., & Michels, J. (2021). Iron based shape memory alloys as shear reinforcement for bridge girders. *Construction and Building Materials*, *274*. https://doi.org/10.1016/j.conbuildmat.2020.121793

Czaderski, C., Weber, B., Shahverdi, M., Motavalli, M., Leinenbach, C., Lee, W., Brönnimann, R., & Michels, J. (2015). Iron-based shape memory alloys (Fe-SMA)-a new material for prestressing concrete structures. *SMAR 2015 - Third Conference on Smart Monitoring Assessmente and Rehabiliation of Civil Structures*.

De Lorenzis, L., & Nanni, A. (2001). Shear Strengthening of Reinforced Concrete Beams with Near-Surface Mounted Fiber-Reinforced Polymer Rods. *ACI Structural Journal*, 60–68.

De Lorenzis, L., & Teng, J. G. (2007). Near-surface mounted FRP reinforcement: An emerging technique for strengthening structures. *Composites Part B: Engineering*, *38*(2), 119–143. https://doi.org/10.1016/J.COMPOSITESB.2006.08.003

Desroches, R., Asce, M., Mccormick, J., & Delemont, M. (2004). Cyclic Properties of Superelastic Shape Memory Alloy Wires and Bars. *Journal of Structural Engineering*, *130*(1), 38–46. https://doi.org/10.1061/(ASCE)0733-9445(2004)130:1(38)

Echegaray-Oviedo, J., Navarro-Gregori, J., Cuenca, E., & Serna, P. (2017). Modified push-off test for analysing the shear behaviour of concrete cracks. *Strain*, *53*(6), e12239. https://doi.org/10.1111/STR.12239

El-Tawil, S., & Ortega-Rosales, J. (2004). Prestressing concrete using shape memory alloy tendons. *ACI Structural Journal*, *101*(6), 846–851.

European Committee for Standardization. (2004). *EN 1992-1-1: Eurocode 2: Design of concrete structures - Part 1-1: General rules and rules for buildings*.

Fédération internationale du béton. (2010). *Shear and punching shear in RC and FRC elements: Technical Report*.

Federation of Canadian Municipalities. (2019). *The 2019 Canada Infrastructure Report Card*.

Ghafoori, E., Hosseini, E., Leinenbach, C., Michels, J., & Motavalli, M. (2017). Fatigue behavior of a Fe-Mn-Si shape memory alloy used for prestressed strengthening. *Materials and Design*, *133*, 349–362. https://doi.org/10.1016/j.matdes.2017.07.055

González-Góez, M., Hrynyk, T. D., & Kim, E. (2023). *Strengthening Shear-Damaged Reinforced Concrete Beams Using Iron-Based Shape Memory Alloys* (pp. 107–119). https://doi.org/10.1007/978-3-031-34159-5_8

Grandić, D., Šćulac, P., & Grandić, I. Š. (2015). Shear resistance of reinforced concrete beams in dependence on concrete strength in compressive struts. *Tehnicki Vjesnik*, *22*(4), 925–934. https://doi.org/10.17559/TV-20140708125658

Guo, Y. F., Wang, Y. S., Zhao, D. L., & Wu, W. P. (2007). Mechanisms of martensitic phase transformations in body-centered cubic structural metals and alloys: Molecular dynamics simulations. *Acta Materialia*, *55*(19), 6634–6641. https://doi.org/10.1016/J.ACTAMAT.2007.08.018

Heo, Y. U., Takeguchi, M., Furuya, K., & Lee, H. C. (2009). Transformation of DO24 η-Ni3Ti phase to face-centered cubic austenite during isothermal aging of an Fe-Ni-Ti alloy. *Acta Materialia*, *57*(4), 1176–1187. https://doi.org/10.1016/J.ACTAMAT.2008.10.056

Hofbeck, J. A., & Mattock, I. O. . I. and A. H. (1969). Shear Transfer in Reinforced Concrete. *Journal Proceedings*, *66*(2), 119–128. https://doi.org/10.14359/7349

Hong, K., Lee, S., Han, S., & Yeon, Y. (2018). Evaluation of Fe-based shape memory alloy (Fe-SMA) as strengthening material for reinforced concrete structures. *Applied Sciences (Switzerland)*, *8*(5). https://doi.org/10.3390/app8050730

Hong, K. N., Yeon, Y. M., Shim, W. B., & Kim, D. H. (2020). Recovery Behavior of Fe-Based Shape Memory Alloys under Different Restraints. *Applied Sciences 2020, Vol. 10, Page 3441*, *10*(10), 3441. https://doi.org/10.3390/APP10103441

Jeong, S., Kim, K. H. E., Lee, Y., Yoo, D., Hong, K., & Jung, D. (2022). Compressive behavior of concrete confined with iron-based shape memory alloy strips. *Earthquake and Structures*, *23*(5), 431–444. https://doi.org/10.12989/eas.2022.23.5.431

Jirsa, J. O., Ghannoum, W. M., Kim, C. H., Sun, W., Shekarchi, W. A., Alotaibi, N. K., Pudleiner, D. K., Zhu, J., Liu, S., & Wang, H. (2017). *Use of Carbon Fiber Reinforced Polymer (CFRP) with CFRP Anchors for Shear-Strengthening and Design Recommendations / Quality Control Procedures for CFRP Anchors*. https://library.ctr.utexas.edu/ctr-publications/0-6783-1.pdf

Leet, K. M., Uang, C.-M., & Joel T. Lanning. (2021). *Fundamentals of Structural Analysis* (Sixth Edition). Mc Graw Hill.

Ma, J., Karaman, I., & Noebe, R. D. (2010). High temperature shape memory alloys. *International Materials Reviews*, *55*(5), 257–315. https://doi.org/10.1179/095066010X12646898728363

Maitenaz, S., Mesnil, R., Onfroy, P., Metge, N., & Caron, J.-F. (2020). Sustainable Reinforced Concrete Beams: Mechanical Optimisation and 3D-Printed Formwork. *Second RILEM International Conference on Concrete and Digital Fabrication Digital Concrete*, 1164–1173.

Mander, J. B., Priestley, M. J. N., & Park, R. (1988). *Theoretical Stress-Strain Model for Confined Concrete*.

Mattock, A. H., & Hawkins, N. M. (1972). Shear Transfer in Reinforced Concrete - Recent Research. *PCI Journal*.

Mohd Jani, J., Leary, M., Subic, A., & Gibson, M. A. (2013). A review of shape memory alloy research, applications and opportunities. *Materials and Design*, *56*, 1078–1113. https://doi.org/10.1016/j.matdes.2013.11.084

Montoya-Coronado, L. A., Ruiz-Pinilla, J. G., Ribas, C., & Cladera, A. (2019). Experimental study on shear strengthening of shear critical RC beams using iron-based shape memory alloy strips. *Engineering Structures*, *200*. https://doi.org/10.1016/j.engstruct.2019.109680

Mörsch, E. (1908). *Reinforced concrete construction, theory and application* (Part 1, Vol. 1). Wittwer.

Ölander, A. (1932). An electrochemical investigation of solid cadmium-gold alloys. *Journal of the American Chemical Society*, *54*(10), 3819–3833. https://pubs.acs.org/sharingguidelines

Otsuka, K., & Shimizu, K. (1986). Pseudoelasticity and shape memory effects in alloys. *International Metals Reviews*, *31*(1), 93–114. https://doi.org/10.1179/IMTR.1986.31.1.93

Precast/Prestressed Concrete Institute. (2010). *PCI Design Handbook* (7th Edition).

Regan, P. E. (1969). Shear in reinforced concrete beams. *Magazine of Concrete Research*, *21*(66), 31–42. https://doi.org/10.1680/MACR.1969.21.66.31

Rius, J. M., Cladera, A., Ribas, C., & Mas, B. (2019). Shear strengthening of reinforced concrete beams using shape memory alloys. *Construction and Building Materials*, *200*, 420–435. https://doi.org/10.1016/j.conbuildmat.2018.12.104

Rizzo, A., & De Lorenzis, L. (2009). Behavior and capacity of RC beams strengthened in shear with NSM FRP reinforcement. *Construction and Building Materials*, *23*(4), 1555–1567. https://doi.org/10.1016/j.conbuildmat.2007.08.014

Rojob, H., & El-Hacha, R. (2018). Performance of RC beams strengthened with self-prestressed Fe-SMA bars exposed to freeze-thaw cycles and sustained load. *Engineering Structures*, *169*, 107–118. https://doi.org/10.1016/j.engstruct.2018.04.009

Rosa, D. I. H., Hartloper, A., de Castro e Sousa, A., Lignos, D. G., Motavalli, M., & Ghafoori, E. (2021). Experimental behavior of iron-based shape memory alloys under cyclic loading histories. *Construction and Building Materials*, *272*, 121712. https://doi.org/10.1016/J.CONBUILDMAT.2020.121712

Santos, P. M. D., & Júlio, E. N. B. S. (2012). A state-of-the-art review on shear-friction. In *Engineering Structures* (Vol. 45, pp. 435–448). https://doi.org/10.1016/j.engstruct.2012.06.036

Schranz, B., Michels, J., Czaderski, C., Motavalli, M., Vogel, T., & Shahverdi, M. (2021). Strengthening and prestressing of bridge decks with ribbed iron-based shape memory alloy bars. *Engineering Structures*, *241*. https://doi.org/10.1016/j.engstruct.2021.112467

Shahverdi, M., Czaderski, C., & Motavalli, M. (2016). Iron-based shape memory alloys for prestressed near-surface mounted strengthening of reinforced concrete beams. *Construction and Building Materials*, *112*, 28–38. https://doi.org/10.1016/j.conbuildmat.2016.02.174

Sharif, A., Al-Sulaimani, G. J., Basunbul, I. A., Baluch, M. H., & Husain, M. (1994). Strengthening of shear-damaged RC beams by external bonding of steel plates. *Magazine of Concrete Research*, *47*(173), 329–334.

Shekarchi, W. A. (2016). *Shear behavior of reinforced concrete bridge pile cap girders strengthened with carbon fiber reinforced polymer (CFRP) strips and CFRP anchors*.

Shin, M., & Andrawes, B. (2010). Experimental investigation of actively confined concrete using shape memory alloys. *Engineering Structures*, *32*, 656–664. https://doi.org/10.1016/j.engstruct.2009.11.012

Soroushian, P., Ostowari, K., Nossoni, A., & Chowdhury, H. (2001). Repair and strengthening of concrete structures through application of corrective posttensioning forces with shape memory alloys: *Https://Doi.Org/10.3141/1770-03*, *1770*, 20–26. https://doi.org/10.3141/1770-03

Standards Australia. (2017). *AS5100.1:2017, Bridge Design*. SAI Global Limited.

Sung, Y.-C., Chang, D. W., Cheng, M. Y., Chang, T. L., & Liu, K.-Y. (2009). *Enhancing the Structural Longevity of the Bridges with Insufficient Seismic Capacity by Retrofitting* (Vol. 1, Issue 1).

Teran, A., & Ruiz, J. (1992). Reinforced concrete jacketing of existing structures. *Earthquake Engineering, 10th World Conference*, 5107–5113.

Vecchio, F. J. (2000). Disturbed stress field model for reinforced concrete: Formulation. *Journal of Structural Engineering*, *126*(9), 1070–1077. https://doi.org/10.1061/(ASCE)0733-9445(2000)126:9(1070)

Vecchio, F. J., & Collins, M. P. (1986). The modified compression-field theory for reinforced concrete elements subjected to shear. *ACI Journal*, *83*(22), 219–231.

Wang, B., & Zhu, S. (2022). Cyclic behavior of iron-based shape memory alloy bars for high-performance seismic devices. *Engineering Structures*, *252*. https://doi.org/10.1016/j.engstruct.2021.113588

Zareie, S., Issa, A. S., Seethaler, R. J., & Zabihollah, A. (2020). Recent advances in the applications of shape memory alloys in civil infrastructures: A review. In *Structures* (Vol. 27, pp. 1535–1550). Elsevier Ltd. https://doi.org/10.1016/j.istruc.2020.05.058

Zhang, Z. X., Zhang, J., Wu, H., Ji, Y., & Kumar, D. D. (2022). Iron-Based Shape Memory Alloys in Construction: Research, Applications and Opportunities. In *Materials* (Vol. 15, Issue 5). MDPI. https://doi.org/10.3390/ma15051723

# Appendix A

# Material characterization results

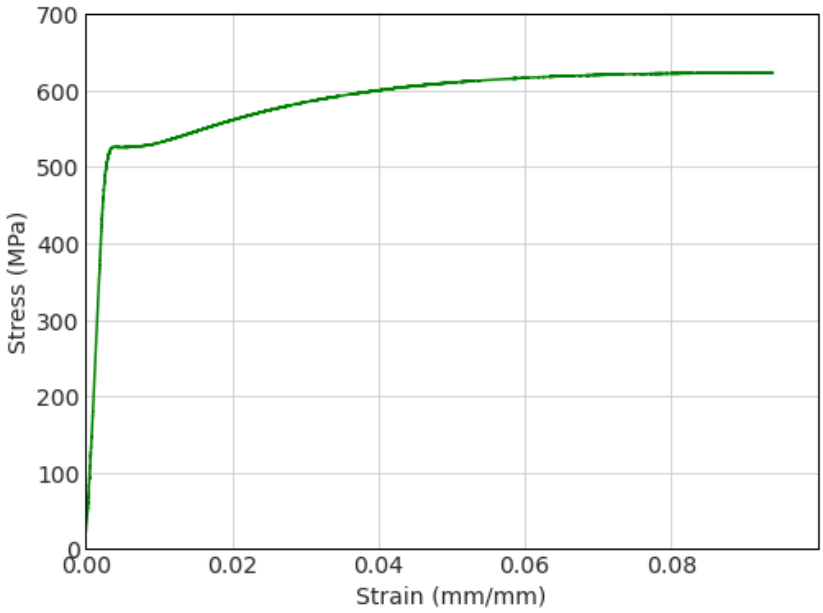



**Figure A.1.** Tensile test 20M rebar

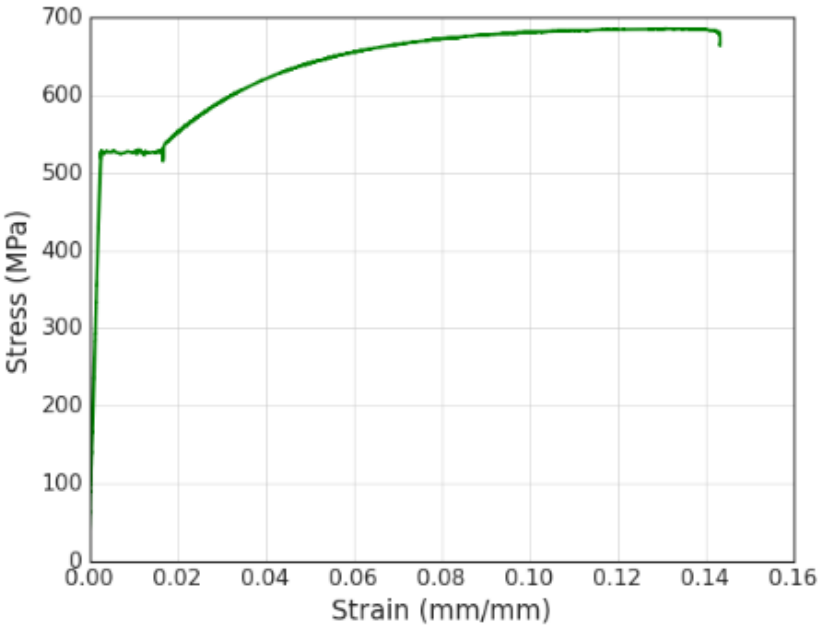



**Figure A.2.** Tensile 10M rebar

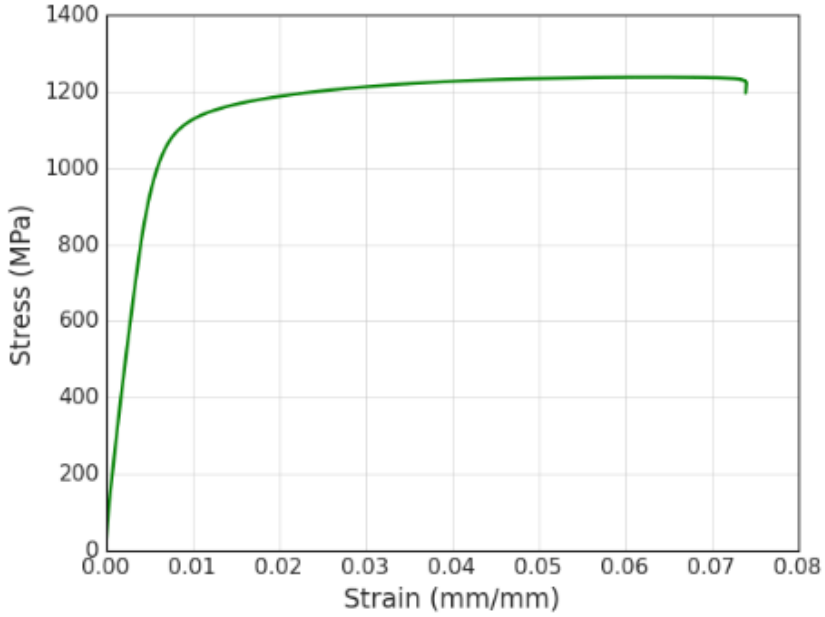



**Figure A.3.** Tensile test 3/16” rebar

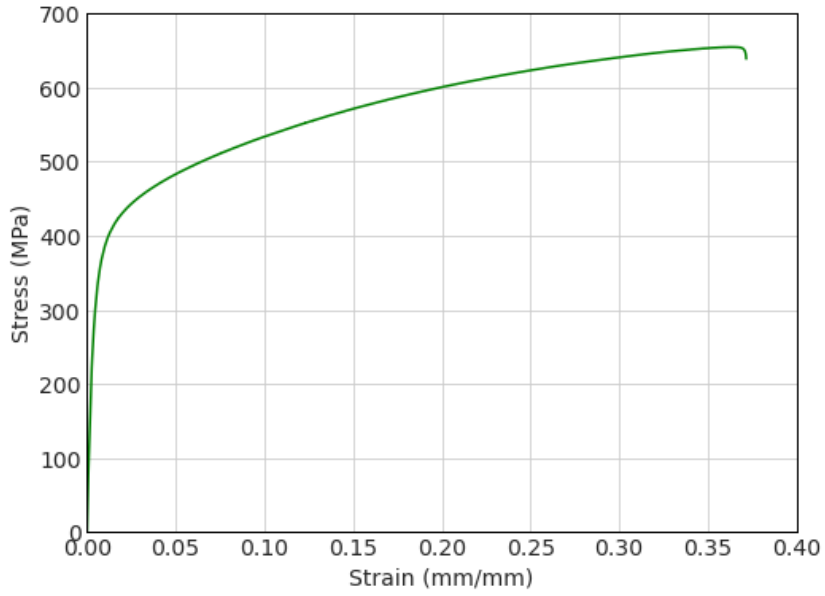



**Figure A.4.** Tensile test Fe-SMA coupon